A COMPARATIVE REVIEW OF PERIDYNAMICS AND PHASE-FIELD MODELS FOR ENGINEERING FRACTURE MECHANICS

A PREPRINT

Patrick Diehl
Center of Computation & Technology
Louisiana State University
Baton Rouge, Louisiana 70803
Email: pdiehl@cct.lsu.edu

Robert Lipton
Department of Mathematics
Center of Computation & Technology
Louisiana State University
Baton Rouge, Louisiana 70808
Email: lipton@lsu.edu

Thomas Wick
Leibniz Universität Hannover
Institut für Angewandte Mathematik
Welfengarten 1, 30167 Hannover, Germany
Email: thomas.wick@ifam.uni-hannover.de

Mayank Tyagi
Craft & Hawkins Department of Petroleum Engineering
Center for Computation & Technology
Louisiana State University
Baton Rouge, Louisiana, 70803
Email: mtyagi@lsu.edu

March 31, 2021

ABSTRACT

Computational modeling of the initiation and propagation of complex fracture is central to the discipline of engineering fracture mechanics. This review focuses on two promising approaches: phase-field (PF) and peridynamic (PD) models applied to this class of problems. The basic concepts consisting of constitutive models, failure criteria, discretization schemes, and numerical analysis are briefly summarized for both models. Validation against experimental data is essential for all computational methods to demonstrate predictive accuracy. To that end, The Sandia Fracture Challenge and similar experimental data sets where both models could be benchmarked against are showcased. Emphasis is made to converge on common metrics for the evaluation of these two fracture modeling approaches. Both PD and PF models are assessed in terms of their computational effort and predictive capabilities with their relative advantages and challenges are summarized.

1 Introduction

Fracturing phenomena in natural and engineered systems is studied extensively experimentally, theoretically, and computationally. Here we focus on two promising approaches: phase-field (PF) and peridynamics (PD) for the computational modeling of fractures in materials. This review is intended as a snapshot capturing in broad strokes the modeling details, assumptions, experimental data sets, and numerical simulations necessary for validation. These methods have the potential to address fundamental issues in complex fracturing with minimal introduction of phenomenological modeling assumptions and numerical tuning parameters. However, systematic comparative analysis for these models, together with validation studies on the set of experiments, are rare. In this review, we attempt to initiate such a comparative analysis and, when possible, invoke validation studies from the experimental literature.

As an example of engineering fracture mechanics application, Hattori et al. (2017) presented a comprehensive comparison of various numerical approaches for the hydraulic fracturing of shale and showed the advantages as well as limitations of many numerical approaches including peridynamics (PD) and phase-field (PF). However, this comparative analysis for various models lacked validation studies on the same set of hydraulic fracturing experiments in order to evaluate predictive capabilities of numerical models. Our review is motivated by the recent workshops on phase-field, peridynamics, and experimental fracture mechanics held at The Banff International Research Station: Hydraulic Fracturing: Modeling, Simulation, and Experiment[1], and the Workshop on Experimental and Computational Fracture Mechanics[2] [1].

The paper is structured as follows: Section 2 introduces the two models and provides a basis on which the models can be compared and contrasted. This summary is an adaptation and extension of the review papers and monograph [2–5] of the two models. Section 3 addresses the fracture physics perspective from the macroscale view. Section 4 attempts to compare the predictive accuracy of the two models for validation against the experimental data. To that end, the Sandia Fracture Challenges data sets were analyzed and computed, the R^2 correlation of relative errors between the simulations and the experiment are presented. Section 5 compares computational aspects of the two models as well as pointing out challenges and opportunities for development. Finally, Section 6 summarizes the modeling capabilities of PD and PF.

2 Overview of models and numerical methodology

This section briefly introduces the two methods, peridynamics (PD) and phase field (PF), respectively. A brief overview of the governing equations, material models, discretizations, numerical analysis, and advanced visualization methods is given. We introduce the ingredients for the comparison of these two models and provide references to the extended literature for the interested reader.

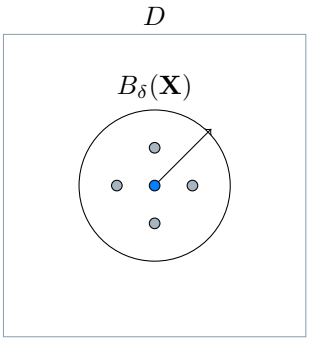

Figure 1: Sketch for the principle of peridynamics where a material point X interacts with its neighbors inside a finite interaction zone $B_\delta(\mathbf{X})$ with the length δ.

2.1 The governing equation of peridynamics

Peridynamics (PD), is a non-local generalization of classical continuum mechanics (CCM), allowing for discontinuities in the displacement field as they arise across cracks. Figure 1 sketches the principle of PD, each material point $\mathbf{X}$ interacts with its neighbors inside a finite interaction zone $B_\delta(\mathbf{X})$ with the length δ. The important feature is that the interaction between the intact material and fractured material is modeled implicitly through a nonlocal field equation that remains the same everywhere in the computational domain. This contrasts with classic fracture theory where, off the crack, the elastic interaction is modeled by the equation of elastodynamics and the fracture set is a free boundary with motion coupled to elastodynamics through a physically motivated kinetic relation. In this way PD models fracture as an emergent phenomena arising from the nonlocal equation of motion. Other nonlocal models exhibiting emergent behavior include the Cucker Smail equation where swarming behavior emerges from leaderless flocks of birds [6–9]. The equation of motion for bond-based peridynamics [10, 11] reads as

$$\varrho(\mathbf{X})\ddot{\mathbf{u}}(t,\mathbf{X}) = \int_{B_\delta(\mathbf{X})} \mathbf{f}(\mathbf{u}(t,\mathbf{X}')-\mathbf{u}(t,\mathbf{X}),\mathbf{X}'-\mathbf{X})d\mathbf{X}' + \mathbf{b}(t,\mathbf{X}), \tag{1}$$

where $\varrho \in \mathbb{R}$ is the material density, $\ddot{\mathbf{u}} \in \mathbb{R}^n$ is the acceleration at time $t \in \mathbb{R}$ of the material point $\mathbf{X} \in \mathbb{R}^n$, $\mathbf{f} : \mathbb{R}^n \times \mathbb{R}^n \times [0,T] \to \mathbb{R}^n$ is the pair-wise force function, $\mathbf{b} \in \mathbb{R}^n$ is an external force density, and $\mathbf{u} \in \mathbb{R}^n$ is the state of deformation at a point in space time, $(t,\mathbf{X})$. Due to the pair-wise interaction in the force function, the material's Poisson ratio is a constraint to $\nu = 1/4$ in three

[1] https://www.birs.ca/events/2018/5-day-workshops/18w5085

[2] http://wfm2020.usacm.org/

dimensions and to $\nu = 1/3$ in two dimensions [12, 13]. To overcome the restriction on the Poisson ratio, multi-point non-local interactions are introduced and this forms the basis for the state-based peridynamic models. The generic state-based peridynamic equation of motion [14] reads as

$$\varrho(\mathbf{X})\ddot{\mathbf{u}}(t,\mathbf{X}) = \int_{B_\delta(\mathbf{X})} (\underline{T}[\mathbf{X},t]\langle \mathbf{X}'-\mathbf{X}\rangle - \underline{T}[\mathbf{X}',t]\langle \mathbf{X}-\mathbf{X}'\rangle) d\mathbf{X}' + \mathbf{b}(t,\mathbf{X}), \tag{2}$$

where the pair-wise force function $\mathbf{f}$ is exchanged with the so-called peridynamic force state $\underline{T} : \mathbb{R}^n \times \mathbb{R}^n \times [0,T] \to \mathbb{R}^n$. A peridynamic state relates to second order tensor, in that both map vectors to vectors. However, in general, it is not a linear or continuous function with respect to $\mathbf{X} - \mathbf{X}'$. For more mathematical details about states in peridynamic, we refer to [14, Section 2].

2.1.1 Damage for PD

The material becomes damaged when the force state at a point $\mathbf{X}$ no longer influences a material point $\mathbf{X}'$ and vice versa. This is modeled by an explicit constitutive law for a material and damage occurs when the difference between deformation states at each point $\mathbf{X}$ and $\mathbf{X}'$ surpass a threshold. The specifics of how this occurs depends on the material model used. For example, for pairwise force functions $\mathbf{f}$ the force acting between two points is often referred to as a bond. When the pairwise force is zero it is said that the bond is broken. Bonds can break irreversibly or alternatively they can heal under the right conditions, this depends upon the material model used.

A common notion for the damage variable $d : [0,T] \times \mathbb{R}^n \to \mathbb{R}$ is the density given by

$$d(t,x) = 1 - \frac{\int_{B_\delta(\mathbf{X})} \mu(t,\mathbf{X},\mathbf{X}')d\mathbf{X}'}{\int_{B_\delta(\mathbf{X})} d\mathbf{X}'} \tag{3}$$

where the scalar function $\mu : [0,T] \times \mathbb{R}^n \times \mathbb{R}^n \to \mathbb{R}$ indicates if the bond between $\mathbf{X}$ and $\mathbf{X}'$ at time t is broken ($\mu = 0$) or active ($\mu = 1$). There are several definitions for the function μ [11, 15–17]. To summarize, the damage variable is the density given by the proportion of intact bonds at time t relative to the total number of bonds inside the neighborhood.

In the remaining part of this section, we will briefly introduce the ingredients of peridynamic models needed for the comparison with the phase field models. For more general details, we refer to [18, 19]. For reviews about PD and the comparison with experimental data we refer to [2, 3].

2.1.2 Material models for PD

Figure 2 shows the tree of different peridynamic material models. The two major material models are bond-based [11, 20–32] and state-based material models. State-based material models are distinguished as ordinary and non-ordinary models. For ordinary state-based PD, the following material models are available: Elastic brittle [14, 33–35], Plasticity [36–38], Composite [39], Eulerian fluid [40], position-aware linear solid (PALS) [41], and Viscoelastic [42–45]. For non-ordinary state-based PD the correspondence model [14, 46], the beam\plate model [47], and a model for cementitious composites [48] are available. For more details we refer to [2].

2.1.3 Discretization methods for PD

Continuous and discontinuous finite element methods [49–51], Gauss quadrature [52], and spatial discretization [11, 53, 54] were utilized to discretize the peridynamic equation of motion. The following implementations are available: Peridigm [55, 56] and PDLammps [53] based on the Message Passing Interface (MPI), NonLocal models [57] based on the C++ standard library for parallelism and concurrency (HPX) [58, 59], and GPU-based codes [60–62]. Three open source implementations of peridynamic Peridigm[3], PDLammps[4], and NonLocalModels[5] are available. One commercial code is available. LS-DYNA provides a bond-based peridynamics implementation discretized with the discontinuous Galerkin FEM [63]. Not to forget one of the first peridynamic implementations, EMU by Stewart Silling using FORTRAN 90 [64].

2.1.4 Numerical analysis for PD fracture models

In this section, we summarize the issues that arise in the numerical analysis of PD fracture models and list the numerical results. The following basic questions for PD fracture models are:

1. Are peridynamic fracture models well-posed, such that unique solutions exist?
2. What is the relation between non-local continuum peridynamic fracture models and their discretizations used in the numerical implementation?
3. How do PD solutions to fracture mechanics problems relate to local fracture models with sharp cracks? Particularly, how does PD relate to the more classical Linear Elastic Fracture Mechanics of continuum mechanics?

These are natural questions to ask, and analogous questions have been investigated and answered for several nonlocal and PD models in the absence of fracture, for this case there is now a vast literature; see [65–83]. This work provides the foundation for the numerical analysis of the PD fracture problem.

[3] `https://github.com/peridigm/peridigm`

[4] `https://lammps.sandia.gov/doc/pair_peri.html`

[5] `https://nonlocalmodels.github.io/`

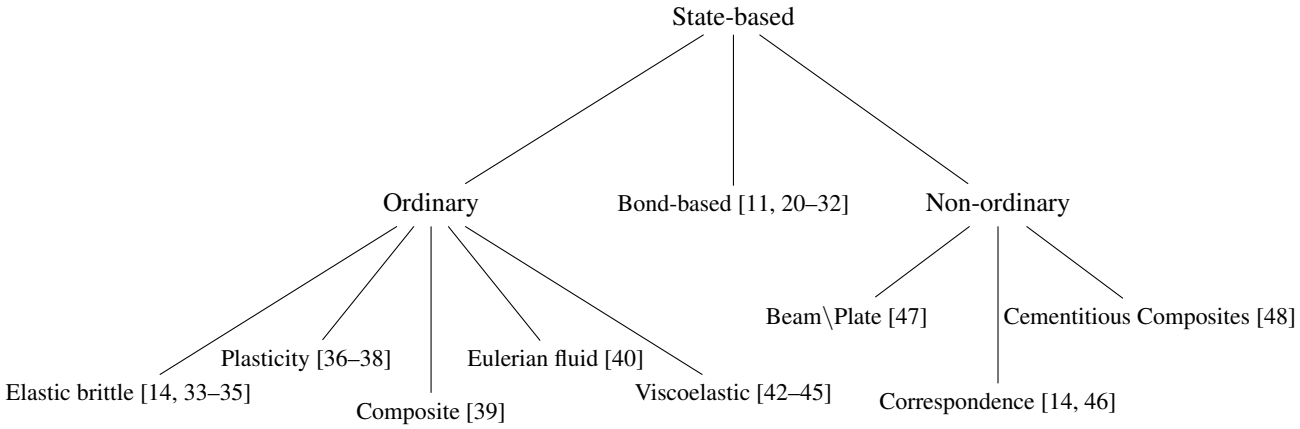

Figure 2: The classification of the different peridynamic material models visualized as a tree. The material models are classified in two major classes: bond-based and state-based material models, respectively. State-based material models are distinguished as ordinary and non-ordinary models. The following ordinary state-based models are available: elastic-brittle, plasticity, composite, Eulerian fluid, and viscoelastic. For non-ordinary state-based models the Beam\Plate, the correspondence model, and a model for cementitious composites are available. Adapted from [2, 3] and extended for this work.

For the case of fracture, the analysis for PD fracture models is still in the initial stages, but meaningful progress has been made, and one can begin to address the three fundamental questions raised in the first paragraph:

First, the answer to question *1)* is addressed. The existence and uniqueness of solutions for peridynamic fracture models have been studied for different classes of constitutive laws. For a simple peridynamic model with with nonlocal forces that soften beyond a critical strain, the existence and uniqueness of the solution over finite time intervals is demonstrated for bond-based and state-based peridynamics in [26, 84, 85]. Energy balance is shown to hold for all times of the evolution. This is a simple constitutive model designed for monotonically increasing loads. A more complex material model with the force degradation law determined by both the time and strain rate for strains above a critical value is considered in [86]. Therein, both existence and uniqueness are established for bond-based peridynamic fracture. The authors [87] address a continuous version of the Prototypical Microelastic Bond (PMB) model introduced by Silling [10]. In this work both existence and uniqueness are shown and the total energy energy of the system is decreasing with time, see [87]. Existence and uniqueness is established for a state-based model with material degradation law, again determined by both the time and strain rate for strains above a critical load in [88]. There, the rate form of energy balance is established among energy put into the system the kinetic energy, elastic energy, and energy dissipated due to the damage. The energy dissipation rate due to damage is seen to be positive. This model is suitable for cyclic loads, see [88]. The theme common to all peridynamic models is that both the existence and uniqueness of solutions follow from the Lipshitz continuity of the peridynamic force and the theory of vector-valued ODE on Banach spaces.

Second, the answer to question *2)* is addressed. The convergence of finite difference approximations to bond-based and state-based peridynamic field theories with forces that soften is established in [89] and [90]. The finite element convergence for bond-based and state-based peridynamic field theories with forces that soften are established in [91] and [50]. A priori convergent rates are linked to the regularity of continuum PD fracture solutions. Existence and uniqueness of solutions in Hölder spaces, and Sobolev spaces H^n, $n = 1, 2$, are proved for both bond and state based force softening models in [50, 90]. The convergence rates for both bond- and state-based models are found to be linear in the mesh size and time step. However the constants appearing in the convergence estimates grow exponentially as the horizon size tends to zero. Fortunately, dynamic fracture experiments last hundreds of microseconds for brittle materials and linear a priori convergence rates for horizons that are tens of times smaller than the sample size are in force for tens of microseconds. Numerical experiments exhibit much better convergence with respect to mesh size and time step thus driving the need for the development of a posteriori estimates for understanding convergence rates.

Third, the answer to question *3)* is addressed. For certain PD models one can theoretically recover a local sharp fracturing evolution. A limiting local evolution is shown to exist for the force softening peridynamic model; see [26, 84]. The limiting local evolution has jump discontinuities in the displacement confined to a set of finite surface areas (more precisely, two-dimensional Hausdorff measure) for almost every time; see [26, 84]. The jump set corresponds to the fracture set in the zero horizon model and the total energy is bounded and given by the classic

energy of linear elastic fracture mechanics [26, 84, 92]. It is shown there that the deformation in the limit model satisfies the local balance of linear momentum equation in quiescent zones away from the crack. Recent work explores the zero horizon limit for straight cracks growing continuously with the goal of capturing the explicit interaction between the growing crack and the surrounding elastic material. For this case, it has been found [93] that the local model obtained in the zero horizon limit is given by a deformation field, that is, the weak solution of the linear wave equation on the domain with the growing crack satisfies the zero traction condition of the sides of the crack. This is in agreement with Linear Elastic Fracture Mechanics (LEFM). Here, the weak solution of the wave equation outside a time-dependent domain defined by a crack was recently developed in [94]. The convergence of PD to the wave equation in time-dependent domains [93] gives theoretical support backing the recent development of new "asymptotically compatible" methods for fracture modeling given in [95]. Lastly, starting with the PD equation multiplying by the velocity and integrating by parts gives the time rate of change of internal energy surrounding the crack front. An applied math argument shows that on passing to the zero horizon limit, the kinetic relation for crack tip growth given by LEFM is recovered, see [96]. Here the classic square root singularity in the elastic field at the crack tip is recovered.

We conclude this section noting that the numerical analysis of PD in the absence of fracture provides compelling heuristics for understanding PD fracture models. Figure 3 illustrates the interplay between horizon length scale and discretization length scale for PD models when local models can be recovered by passing to the the small horizon limit in nonlocal models, see [78, 79]. When a numerical scheme can be designed so that the diagonal arrow captures the same limit as obtained by proceeding along the sides of the square problem, a numerical scheme is said to be asymptotically compatible. This is the motivation behind the numerical approach of [95] to capture the coupling between intact material surrounding a growing crack. For example, if one considers elastic problems in the absence of fracture, then for the diagonal transition where the horizon δ and the nodal spacing h go to zero, it is known that: using piece-wise constant finite elements, the correct local solution is obtained, if the nodal spacing decays faster than the horizon to zero [78]. This is seen for the EMU nodal discretization [64] which converges to the limit $u_{0,0}$ along the diagonal if the nodal spacing decays faster than the horizon [81]. The sensitivity of horizon and nodal spacing are studied in [82, 83].

To conclude, we point out in the absence of fracture, the relation of PD to molecular dynamics (MD) has been shown in [97]. Along another direction, the relation of PD to smooth-particle hydrodynamics (SPH) is established in [77]. With these studies in mind, it is clear that upscaling MD fracture models to PD and establishing the relation between SPH and PD for fracture would be desirable.

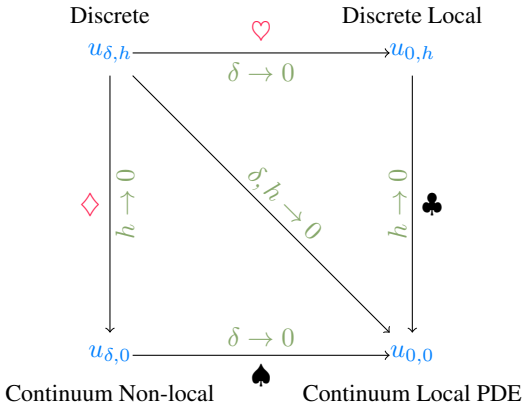

Figure 3: The consistency of non-local models and the limits of the horizon δ and the nodal spacing h [78, 79]. Adapted from [98].

2.1.5 Visualization of PD results

Since peridynamics is a meshless method, information, e.g. stress and strain, are only available on the discrete nodes. Thus, every graphics software, *e.g.* Paraview [99] or VisIt [100], supporting particles can be used to visualize meshless simulation results. However, to understand the simulation and compare against experimental data, this information is needed on a larger scale. First, peridynamic theory was used for physically-based modeling and rendering. Here, the animation of brittle fracture [101], the animation of fractures in elastoplastic solids [102], and the animation of hyper elastic materials [103] were studied. Second, the visualization of fragmentation [104, 105] and visualization of fracture progression [106] were investigated. For more details, we refer the readers to [3].

2.2 Phase-field models governing equations

The theories for phase-field fracture and damage models were introduced by Francfort & Marigo [107] and Aranson et al. [108] and the numerical implementation by Bourdin et al. [109]. We also refer to [110] and the recent review paper [111]. Figure 4a sketches the ingredients to define the phase-field external potential as

$$P(\mathbf{u}) = \int_{\Omega} \mathbf{b}^* \mathbf{u} dV + \int_{\partial\Omega_t} \mathbf{t}^* \mathbf{u} dA \tag{4}$$

where $\mathbf{b}^*$ is the distributed body force. In Figure 4a the domain Ω of the solid with a crack set Γ is considered. For the boundary $\partial\Omega$ of the domain Ω two kinds of boundary conditions along the normal vector $\mathbf{n}$ are considered such that $\partial\Omega_u \cap \partial\Omega_t = \emptyset$. The displacement $\mathbf{u}$ is applied to the $\partial\Omega_u$ boundary and traction $\mathbf{t}^*$ is applied to the $\partial\Omega_t$ boundary. Within phase-field models the crack is defined by a finite thickness in Ω_c around the sharp crack Γ using the so-called phase-field crack function $\phi : \mathbb{R} \to [0, 1]$, see Figure 4b. In this paper, the notation is that $\phi = 1$

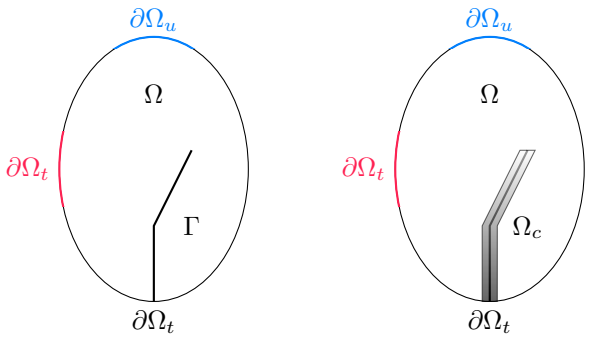

(a) (b)

Figure 4: The solid phase-field domain Ω with (a) a sharp crack interface Γ and (b) the approximated crack using the phase-field crack function ϕ resulting in a regularized crack representation Ω_c.

indicates damage and $\phi = 0$ means intact material (some authors define it the other way around). Between $\phi = 0$ and $\phi = 1$, the function varies smoothly with values $0 < \phi < 1$, which is the so-called transition zone. Consequently, the sharp crack defined on Γ is regularized by a domain integral defined on Ω_c. The approximated surface energy reads as

$$\psi_c(\Gamma) = \int_\Gamma G_c dA \approx \int_{\Omega_c} G_c \gamma(\phi, \nabla\phi) dA \text{ with} \tag{5}$$

$$\gamma(\phi, \nabla\phi) = \frac{1}{2}\left[\frac{1}{l_0}\phi^2 + l_0|\nabla\phi|^2\right] \tag{6}$$

with G_c as the critical energy release rate, $\gamma(\phi, \nabla\phi)$ as the so-called crack surface density function as in [112] (mathematically this is an Ambrosio-Tortorelli elliptic approximation [113, 114]), and $l_0 > 0$ is the so-called length scale (i.e., regularization) parameter. Moreover, l_0 characterizes the width of the regularized domain Ω_c. Note that there are other formulations for the crack surface density function available [115, 116]. The "bulk" strain energy can be extended to the entire domain by regularizing the sharp crack interface. It holds

$$\psi_s(\mathbf{u}, \phi) = \int_{\Omega\cup\Omega_c} g(\phi)\psi_0(\epsilon(\mathbf{u}))dV \tag{7}$$

where ψ_0 is the so-called non-degraded bulk strain energy and $g(\phi)$ the so-called degradation function. Usually, $g(\phi) = \varphi^2 + \kappa$ or $g(\phi) = (1-\varphi^2) + \kappa$ with a small $\kappa > 0$, which can be justified with [113, 114]. A family of degradation functions and their numerical justification was done in [117]. The mathematical relation between l_0 and κ is linked to Γ convergence in which $l_0 \to 0$ and $\kappa \to 0$ with the asymptotic behavior $\kappa = o(l_0)$; see e.g., [118] and again the approximation results in [113, 114] and for the first numerical realization of phase-field (variational) fracture, we refer to [109].

Thus, the total energy in the entire domain $\Omega\cup\Omega_c$ is given by

$$E(\mathbf{u}, \phi) = \int_{\Omega\cup\Omega_c} g(\phi)\psi_0(\epsilon(\mathbf{u}))dV + \int_{\Omega\cup\Omega_c} G_c\frac{1}{2}\left[\frac{1}{l_0}\phi^2 + l_0|\nabla\phi|^2\right]dV - P(\mathbf{u}). \tag{8}$$

Several general types of Ψ_0 functions have been proposed, and it was shown that a suitable choice could avoid nonphysical growth of cracks under compressive loading [119]. For more details we refer to [4, 120]. Moreover, in most studies, as model assumption from a physics perspective, the crack cannot heal, and therefore the above energy functional is subject to a crack irreversibility (an entropy condition), which is mathematically expressed as an inequality constraint in time or quasi-static loading:

$$\partial_t\phi \geq 0.$$

Due to this constraint, we deal with a quasi-static (time-dependent) nonlinear, coupled variational inequality system.

2.2.1 Properties of ϕ and crack interface reconstruction

It can be rigorously proven with cut-off arguments that $\phi \in [0, 1]$; see for instance [121], which follows from the definition of the Ambrosio-Tortorelli functional and the regularization of the total energy. When further terms (physics) are added, the property $\phi \in [0, 1]$ may get lost, and one must argue carefully. For instance, in pressurized fractures, the pressure can have positive and negative values and, therefore, further cut-off arguments are necessary in order to establish the bounds for ϕ [122]. As the second topic in this short paragraph, we want to mention the principal idea when the crack interface must be known explicitly. Due to the regularization using ϕ, there is some liberty as to when the exact crack interface must be known. In these cases, the phase-field function is interpreted as a level-set function ([123]) and the crack interface is, for instance, chosen as $\phi_c := \phi = c_I$ with for example $c_I = 0.2$ [5, 124, 125].

2.2.2 Brief review of some theoretical findings

We briefly list some important well-posedness results. In [126] first existence results for quasi-brittle fracture of the original model by Francfort & Marigo [107] were shown for the antiplane setting for scalar-valued displacements. In [127] the existence and convergence of quasi-static evolutions for the vector-valued case were established. Shortly after, the existence of quasistatic crack growth in nonlinear elasticity was proven [128]. The existence of solutions for dynamic fracture using Ambrosio-Tortorelli [113, 114] approximations was established in [129]. Since crack initiation is an important topic within phase-field based crack models, we mention theoretical

work by Chambolle et al. [130], Goethem/Novotny [131], and recently Kumar et al. [132]. Some theoretical findings on the crack path were provided in [133]. For mode III dynamic fracture modeled using [134], one can follow a sequence of solutions as $l_0 \to 0$, to obtain existence of a limiting displacement with bounded Linear Elastic Fracture Mechanics energy [26]. The latest review of the original model, in terms of the sharp crack approximation (without phase-field, but nonetheless the ground basis of regularized models such as phase-field) can be founded in recently published article by Francfort [135]. Furthermore, we refer to the SIAM News article [111].

2.2.3 Fracture/damage models for PF

Table 1 lists the available phase-field fracture and damage models. The following models have been developed within the phase-field framework: fatigue [136–140], multi-field fracture [115, 141–156], plate/shell fracture [112, 146, 157–164], three-dimensional fracture [112, 146, 157–164], finite deformation fracture [163, 165–170], dynamic fracture [134, 157, 158, 171–175], cohesive fracture [110, 176–179], ductile fracture [143, 161, 180–184], anisotropic surface energy [185–190], and layered material fracture [178, 191–198].

Furthermore, we summarize various models for splitting the energy (i.e., strain / stress) into different parts for accounting the fracture growth behavior under tension and compression. To the best of our knowledge, we are aware of Amor et al. [199], Miehe et al. [112], Zhang et al. [200], Strobl/Seelig [201], Steinke/Kaliske [202], Bryant/Sun [203], Freddi/Royer-Carfagni [204], Bilgen/Homberger/Weinberg [205], and Fan et al. [206].

2.2.4 Treating the crack irreversibility constraint

For treating the irreversibility constraint $\partial_t \phi \geq 0$, five fundamental procedures have been proposed:

1. Fixing crack nodes by Dirichlet values [109, 215];
2. Strain history function [216];
3. Penalization: simple and augmented Lagrangian [122, 217];
4. Primal-dual active set methods [218];
5. Complementarity system with Lagrange multipliers as unknowns [208];
6. Interior-point methods [219].

Comparisons of some of these approaches were performed in [220] and [5].

2.2.5 Discretization, Solvers, and Software for PF

Classical Lagrange Galerkin finite elements, mixed formulations, discontinuous finite elements, exponential shape functions, or isogeometric elements were mostly utilized for the spatial discretization of the fracture/damage models as described in the previous section. For discretized nonlinear systems, the following solvers are available: alternating minimisation algorithms [109, 116, 173, 199, 221–224], alternating minimisation algorithm with path-following strategies [225], staggered scheme [216], stabilized staggered schemes [226–229], monolithic solvers [5, 112, 218, 230–234], and monolithic solvers with path-following strategies [235, 236].

For solving linear equation systems, most often black-box (direct) solvers have been adopted. Only recently [223] proposed conjugate gradient (CG) solutions with multigrid preconditioning for the decoupled phase-field displacement system. For monolithic solvers, a generalized minimal residual (GMRES) method with parallel algebraic multigrid preconditioning was proposed in [237]. A matrix-free geometric multigrid preconditioner was developed in [233], and its parallelized variant in [238].

Following proprietary implementations using Matlab [239, 240], COMSOL [241], [242, 243] using FEAP[6], and Abaqus [162, 244–248] are available. Following open source implementations: [236] using Nutils [249], [177] using JIVE[7], [250] using MOOSE [251], [252] (pfm-cracks[8] based on deal.II) and [253] using deal.II[9], and [173, 223] using FENICS [254] are available. In addition a GPU-based implementation [255] and the MEF 90 Fortran implementation [107, 110, 222, 256] are available.

2.2.6 Numerical analysis for PF

A posteriori error estimation For numerical analysis with respect to a posteriori error estimation, a short summary is presented here. First, work on residual-based error estimators goes back to [221, 257]. Extracting error indicators for local mesh refinement based on an a posteriori error estimator for the phase-field variational inequality realizing the fracture irreversibility constraint are presented in [258]. The development of goal-oriented mesh adaptivity was undertaken in [5, 259]. The Ambrosio–Tortorelli functional is used to Γ approximate each time evolution step in [260]. An additional penalty constraint is enforced for the irreversibility of the fracture as well as the applied displacement field. An a posteriori error estimator driving the anisotropic adaptive procedure is utilized for mesh adaptivity. According to the authors, the main properties of automatically generated meshes are to be very fine and strongly anisotropic in a small neighborhood region of the crack, but only far away from the crack tip, while they show a highly isotropic behavior in a neighborhood of the crack tip instead. The Ambrosio–Tortorelli functional is applied in [221] for two adaptive finite element algorithms for the computation of its (local) minimizers. Two theoretical results demonstrate convergence

[6] `http://projects.ce.berkeley.edu/feap/`
[7] `http://www.jem-jive.com`
[8] `https://github.com/tjhei/cracks`
[9] `https://www.dealii.org/`

Table 1: Overview of various fracture and damage models available for phase-field modeling. Adapted and extended from [4]

fracture/damage models	
ductile fracture	[143, 161, 180–184]
cohesive fracture	[110, 175–179, 207]
dynamic fracture	[134, 157, 158, 171–173]
fracture in incompressible solids	[208, 209]
finite deformation fracture	[163, 165–169]
3D fracture	[112, 146, 157–164]
plate/shell fracture	[168, 191, 210–213]
plate/shell fracture	[168, 191, 210–213]
multi-field fracture	[115, 141–154, 214]
fatigue	[136–140]
layered material fracture	[178, 191–198]
anisotropic surface energy	[185–190]

of the developed algorithms to the local minimizers of the Ambrosio–Tortorelli functional. However, the Ambrosio–Tortorelli functional is for quasi-static simulations and might not apply to dynamic fracture situations. The phase-field parameter itself is used in [261] to refine the mesh. The gradients of the phase-field are high in the near crack region and close to one away from the crack. A threshold is introduced to run the dynamic phase-field simulation for a few time steps, then all elements are refined above the introduced threshold, and the simulation is resumed with the newly refined mesh. This procedure is repeated until the convergence criterion is met.

It is expected that improved error estimates can further advance both PD and PF modeling approaches to pave the path for routine use as predictive simulations for a certain class of fracture problems.

Goal functional evaluations and computational analysis for $\epsilon - h$ relationship In [5, 259] a slit domain (a square plate with an initial crack) with displacement discontinuity at the crack and the manufactured displacement field [262, 263] are utilized to study the $\epsilon - h$ relationship. Note that the crack in this study is represented by the phase-field damage function ϕ. Motivated by [118, 264], various simulations for $\epsilon = ch^l$ with $l \in (0, 1]$ and h as the mesh size are conducted. Three cases of mesh refinement are studied: *1)* $c = 2.0$ and $l = 1.0$, *2)* $c = 0.5$ and $l = 0.5$, and *3)* $c = 0.5$ and $l = 0.25$. First, the influence of ϵ on the goal function evaluation is considered. Therefore, the goal function $J(u_{\text{FM}}) := u_{\text{FM}}(0.75, -0.75)$ for a displacement point value is utilized which results in the total error $J(u_{\text{FM}}) - J(u_h)$. The maximal convergence order of $r = \mathcal{O}(\epsilon)$ was obtained in case *2)* where $r = \epsilon = 0.5$. The observed order is $r = \epsilon = 0.25$ for case *3)* and $r \approx 0.9 < \epsilon$ for case *1)*. These results lead to the assumption that $|J(u_{\text{FM}}) - J(u_h)| = \mathcal{O}(\epsilon)$ as presented in [146, 218, 226, 237]. In addition, two phase-field fracture configurations were proposed as prototype models for comparison in the recent benchmark collection [265].

Adaptivity Regarding adaptivity, we distinguish between spatial and temporal mesh refinement and adaptive multiscale approaches. Spatial mesh refinement goes back to anisotropies introduced by the mesh [266], residual-based adaptive finite elements [221, 257], anisotropic adaptive mesh refinement [260], and pre-refined meshes where the crack path is known a priori [158]. Other computational convergence analyses were undertaken in [267]. For unknown crack paths, a predictor-corrector approach was developed and applied in [146, 218, 268], goal-oriented error-control [259], and mesh refinement in multiscale phase-field methods [269]. A few rigorous studies on temporal error control exist [255, 270]. Apart from classical mesh refinement, an adaptive predictor-corrector non-intrusive global-local (multiscale) approach [240] was developed based on the approach presented in [271], was applied to porous media [272], and extended to multilevel concepts [273].

Solver analyses Using alternating minimization for solving the coupled displacement-phase-field problem, the convergence of the scheme was established in [222] and [221]. A convergence proof for a truncated nonsmooth Newton multigrid method was very recently undertaken in [274]. For further fully-coupled (i.e., monolithic) techniques, no rigorous convergence are available, but significant numerical evidence of the performance of nonlinear solvers [5, 112, 218, 219, 230–236].

Zhang et al. [275] used a length scale material parameter to evaluate the accuracy of phase-field modeling of brittle fractures with available experimental data. They observed significant discrepancies between numerical predictions and the experimentally observed load-displacement curves after the critical force, despite a reasonably accurate prediction of crack paths. Zhuang et al. [276] implemented the phase-field method in a staggered scheme to sequentially solve for the displacement, phase-field, and fluid pressure. Asymmetric deflection along material interfaces and penetration of hydraulic fractures in naturally-layered porous media were reported

for different layer arrangements based upon their respective stiffness as measured by E and G_c. Farrell and Maurini [223] reformulated the alternate minimization algorithm for the variational fracture approach to simulate nucleation and propagation of complex fracture patterns as a nonlinear Gauss-Seidel iteration along with over-relaxation to accelerate its convergence. They showed further reduction in solution time by utilizing the accelerated alternate minimization with Newton's method. Brun et al. [226] showed a iterative staggered scheme, a two-field variational inequality system with independent phase-field variable and displacement variables. For the convergence using a fix-point argument and a natural condition, the elastic mechanical energy remains bounded and with a sufficiently thick diffusive zone around the crack surface, monotonic convergence is achieved. Noll et al. [277] presented results for ductile fracture with linear isotropic hardening and discussed the computational costs for 3D simulations while analyzing added computations due to mesh refinement. Chukwudozie et al. [278] presented a unified fracture-porous medium hydraulic fracturing model that handled interactions among multiple cracks, as well as the evolution of complex crack paths in 3D simulations using energy minimization without any additional branching criterion, but the location of crack tip and its velocity remains a challenge in complex configurations. Further detailed linear solver analyses for quasi-monolithic phase-field fracture using a GMRES solver with matrix-free geometric multigrid preconditioning were conducted in [233]. Scalability tests of parallel performance were performed in [237] and [238].

It is evident that further improvements in robust solvers will be the key for both PD and PF approaches to be adopted as the engineering tools of choice to predict fracture phenomena.

3 Macroscale View of Crack Propagation Physics using Thermodynamics Constraints and Constitutive Relationships

According to Haslach [279], a maximum dissipation non-equilibrium evolution model can describe the unsteady crack propagation rate for both brittle fracture and for viscoplastic behavior at the crack tip. Ulmer et al. [280] presented a thermodynamically consistent framework for phase-field models of crack propagation in ductile elastic-plastic solids under dynamic loading with an incremental variational principle and validated it against the classical Kalthoff-Winkler experimental results. Mauthe and Miehe [281] used two constitutive functions – free energy and dissipation potential to incorporate fluid flow in cracks during hydraulic fracturing and coupled it to a phase-field approach to fracture within a variational framework. Miehe et al. [282] proposed a gradient damage formulation with two independent length scales to regularize the plastic response and the crack discontinuities to ensure that the damage zones of ductile fractures remain inside of plastic zones. Roy et al. [283] presented a rephrased phase-field theory of continuum damage in a peridynamics setup and showed promising results of mode II delamination. Farrahi et al. [284] demonstrated that under mode I crack growth and proper calibration of parameters, PFM always agreed with Griffith's theory.Alessi et al. [285] demonstrated that macroscopic responses assimilable to brittle fractures, cohesive fractures, and a sort of cohesive fracture, including depinning energy contributions by tuning a few key constitutive parameters such as relative yield stresses and softening behaviors of the plasticity and damage criteria. It is duly noted that both PD and PF show promise to visualize and predict complex fracture phenomena without resorting to ad-hoc modeling assumptions.

4 Validation against experimental data

The validation against experimental data is a cornerstone to access the predictive accuracy of any engineering fracture mechanics model. In this section, the experiments used as benchmarks for peridynamic models are compared against the ones used as benchmarks for phase-field models. We limited the focus to the Sandia Fracture Challenge and publications where both models were compared to the same experimental data. Experimental data from Jeffery and Bunger (2009) could also be used for validation of different numerical simulators for hydraulic fracture propagation. For a detailed review about the comparison with experimental data, we refer to [3] for peridynamic models and for phase-field models to [4, Section 2.12].

The Sandia Fracture Challenge is considered to showcase the accuracy of the two models for various complex experimental data. For the first and third fracture challenge, we could find the contributions of peridynamic models, see Section 4.1 and Section 4.2, respectively. No studies using phase-field models were found for all three fracture challenges. The summary of model accuracy is shown in Table 4.

The comparison with the same experimental data is listed in Section 4.3. The overview of the accuracy for the comparison with the same experimental data is summarized in Table 5. For all compared values, following error measurements were calculated: For scalar values, the relative error $\epsilon_{\text{rel}} = {}^{(x_{\text{sim}} - x_{\text{exp}})}/_{x_{\text{exp}}}$ and for a time series the coefficient of determination R^2 [286] is computed, when applicable. The coefficient of determination R^2 is defined as

$$R^2 = 1 - \frac{SSE}{SST} \tag{9}$$

for two series of n values $y_1, \ldots, y_n$, the so-called series of observables and $\hat{y}_1, \ldots, \hat{y}_n$, the so-called series of pre-

dictions. Where the total sum of squares SST reads as

$$SST = \sum_{1}^{n}(y_i - \overline{y})^2 \quad \text{with} \quad \overline{y} = \frac{1}{n}\sum_{1}^{n} y_i \tag{10}$$

and the sum of square residuals (or errors) reads as

$$SSE = \sum_{1}^{n}(y_i - \hat{y}_i)^2. \tag{11}$$

Thus, R^2 is a statistical measure in the range of zero to one to indicate how good the series of predictions $\hat{y}_i$ approximates the series of observables y_i. $R^2 = 1$ implies that $SSE = 0$ and therefore, the series of observables fits the series of predictions perfectly. If $R^2 = 0$ and therefore $SSE = SST$ then the mean of observables series is as good as any predicted series. For the time series the WebPlotDigitizer[10] was used to extract the x and y coordinates of the respective plot from the Sandia report. The `scipy.stats.linregress`[11] functionality of the python SciPy package [287] was utilized to compute the R^2 correlation.

4.1 First Sandia Fracture Challenge

In the first Sandia Fracture Challenge [288] blind round robin predictions of ductile tearing for an alloy (15-5PH) were studied. The stress-strain curve of a tensile bar was provided to calibrate the model. Experiments on CT specimens were conducted and the extracted quantities of interest are shown in Figure 5. The geometry has a blunt notch A and three holes B, C, and D, respectively. The two unlabeled holes were used for the load pins to apply the load in force $\pm F$. The following three challenge questions were used for predictive simulations:

1. What is the load force and the COD displacement at the time of the crack initiation?
2. What is the path of crack propagation?
3. At what force and COD displacement does the crack re-initiate out of the first hole, if the the crack does propagate to either holes B, C, or D?

and the teams had to answer these questions with their respective model. Team 9 from the University of Arizona used a bond-based peridynamic model [10, 11] to answer these questions. During the ten experiments the crack path $A - D - C - E$ occurred nine times and the crack path $A - C - E$ occurred one time. Team 9 predicted the second path in their simulations as the answer to the second question. Table 2 shows the answers to the remaining questions. The first row shows the average value for the force (N) and the crack open displacement (COD) ((mm)) for the first crack event and the second crack event. The first value in every column is the value obtained by the load drop and the second one the visual obtained value. The second row contains the average value obtained by the simulations of team 9. The relative error ϵ_{rel} for the 1st crack events are for the force $-0.4/-0.28$ and for the COD $-0.7/-0.7$ respectively. The relative error for the 2nd crack events are for the force $-0.31/-0.2$ and for the COD $-0.7/-0.7$ respectively.

Table 2: The average values of the force (N) and the crack opening displacement (COD) (mm) for the crack path $A - C - E$, see Figure 5. For the experiments the average value obtained by the load drop is shown first and the visual obtained value, second. For the simulations of team 9, their obtained average value is shown. Adapted from [288].

	1st crack event		2nd crack event	
	Force (N)	COD (mm)	Force (N)	COD (mm)
Exp	8066/6621	3.542/3.538	5128/4363	5.217/5.362
PD	4782	1.092	3514	1.575

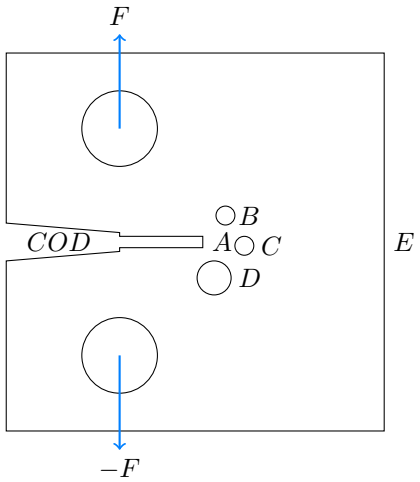

Figure 5: Simplified geometry of the CT specimen to sketch the experimental quantity of interests which the peridynamic simulation was compared against. Adapted from [288].

4.2 Third Sandia Fracture Challenge

In the third Sandia Fracture Challenge, the predictions of ductile fracture in additively manufactured metals were studied. The data of tensile tests was provided to calibrate the simulation models. Figure 6 shows a simplified sketch of the geometry to showcase the following challenge questions for predictive simulations:

1. What is the force at the displacements 0.25, 0.5, 0.75, and 1.0 mm?
2. What is the force and Hencky (logarithmic) strain in the vertical direction of the points $P1$–$P4$ on the surface at the following forces: 75%

[10] `https://automeris.io/WebPlotDigitizer/`

[11] `https://docs.scipy.org/doc/scipy-0.15.1/reference/generated/scipy.stats.linregress.html`

Table 3: Comparison of the measurements and the obtained loads in the simulations for four different displacements. For the comparison the nominal load is considered. Adapted from [291].

Force (kN) for four displacements (mm)				
	0.25	0.5	0.75	1.0
Exp	7.884	8.164	8.203	6.538
PD	7.469	6.919	4.330	2.188

and 90% of peak load (before peak), at peak load, and 90% after the peak load?

3. What is the force versus the gauge displacement for the test?
4. What is the force and Hencky (logarithmic) strain in the vertical direction of the points $P1$–$P4$ on the surface over time?
5. What is the force and Hencky (logarithmic) strain in the vertical direction of the lines $H1$–$H4$ on the surface at the the same forces as in questions 2?

Team C from the University of Texas Austin used an explicit peridynamic model with bond damage. The answers to question 1 are shown in Table 3. The relative errors are: -0.05, -0.15, -0.47, -0.66, respectively. The R^2 correlation for question 3, load (kN) vs displacement (mm) is 0.7. For the relative errors with respect to question 2, one can only look at the trend at the peak load, since all other loads were defined relatively to it. For the peak load, a relative error of -0.08 was reported. The relative errors for the vertical logarithmic strain (%) for point $P2$ are 7, 4.8, -0.8, and -0.8, respectively. The R^2 correlation at the peak load for the Hencky strain on lines $H3$ for question 4 is 0.44. Unfortunately, we had issues extracting the R^2 correlations for line $H4$ with our tools. Note that this was a blind verification, and the same team performed a revisited simulation with more details, receiving better results [289]. However, phase-field simulations were done only qualitatively using the geometry of the third Sandia Fracture Challenge [290].

4.3 Comparison of both models with the same experimental data

First, finite elastic deformation and rupture in rubber-like materials [292] was studied for phase-field models in [293] and for peridynamic models in [294]. In these publications, a rubber sheet with double edge notches was studied. For the experimental setup the length of the notches a varied from, 12mm, 16mm, 20mm, and 24mm. The applied displacement (mm) vs the reaction force (N) was compared for the one observed in the experiment and the one obtained in the simulations. The R^2 correlation for PD are: 0.83, 0.99, 0.98, 0.98, 0.98, and 0.78 respectively. The R^2 correlation for PF are:

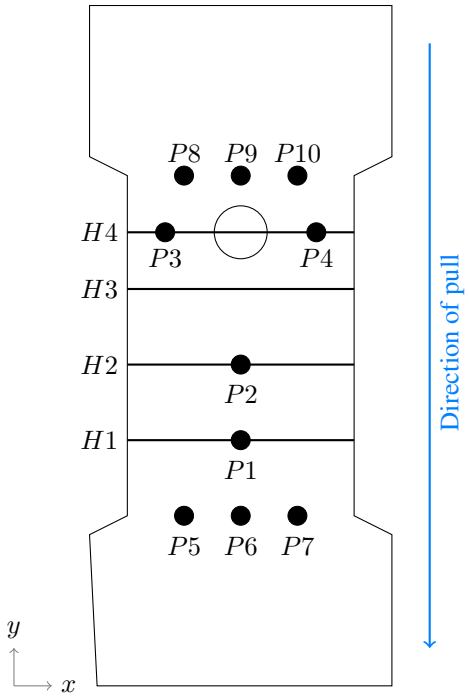

Figure 6: Simplified sketch of the geometry to showcase the quantity of interests for the fracture challenge. Adapted from [291].

0.78, 0.84, 1, 0.64, and 0.65 respectively.

Second, dynamic brittle fracture in glassy materials was studied in [295, 296]. In this study, a phase-field model [216], a discontinuous-Galerkin implementation of PD [297], and a meshfree discretization of PD [11] are used. For all three implementations, the crack angle after branching, the time of crack branching, and position of the crack branching were compared with the experimental results. In this study various discretization parameters were studied, however, we report the discretization parameters corresponding to the best agreement with the experimental data. First, the value for the meshfree discretization is presented, followed by the value for the discontinuous-Galerkin discretization, and the value for the phase-field model last. The relative errors for the crack angle are: -0.21, -0.35, and -0.51, respectively. The relative errors -0.06 for the event of crack branching in time are the same for all simulations. The relative errors for the crack branching position are: 0, -0.12, and 0, respectively.

5 Comparison between peridynamics and phase-field fracture models

In this section, the two approaches PD and PF are compared with respect to their computational aspects, advantages in simulating complex fracture phenomena, and the challenges faced by these numerical methods.

Table 4: Overview of the Sandia Fracture Challenge with contributions of peridynamic models. Two different research groups contributed to the first and second Sandia Fracture Challenge using a peridynamic model. To the best knowledge of the authors, no phase-field model contributed to the Sandia Fracture Challenge. However, phase-field simulations where done using the geometry of the third Sandia Fracture Challenge [290]. To compare with the experimental measurement, the relative error is provided for scalar values, and the R^2 correlation for a series of values. For the first Sandia Fracture Challenge, the following quantities were studied: *a)* Force (N) 1st crack event, *b)* Crack Opening Displacement (COD) (mm) 1st crack event, *c)* Force (N) 2nd crack event, and *d)* COD (mm) 2nd crack event. For the third Sandia Fracture Challenge, the following quantities were studied: *a) - d)* Force (kN) at 0.25, 0.5, 0.75, and 1 mm displacement; *e)* Force vs displacement (time series); *f)* Force (kN) at Peak load; and *g)* Hencky strain (%) on line $H3$ at peak load.

	First Sandia Fracture Challenge [288]				Third Sandia Fracture Challenge [291]						
	a	b	c	d	a	b	c	d	e	f	g
ϵ_{rel}	$-0.4/-0.28$	-0.7	$-0.31/-0.2$	-0.7	-0.05	-0.15	-0.47	-0.66		0.08	
R^2									0.7		0.44

Table 5: For the two experiments, phase-field and peridynamic models were used for comparison.To compare with the experimental measurement, the relative error is provided for scalar values and the R^2 correlation for a series of values. For the double edge notches the displacement (mm) vs the reaction force (N) was compared for a initial crack lengths 12, 16, 20, 24, and 28mm, see *a) - d*. For the dynamic brittle fracture in glassy materials following quantities were studied: *a)* crack angle, *b)* crack branching position, and *c)* crack branching event. Here, two different PD discretizations: a meshfree discretion [11] and a discontinuous-Galerkin implementation [297]. For each error measurement, the first value is with respect to the meshfree discretization, and the second one with respect to the discontinuous-Galerkin implementation

Double edge notches						Dynamic brittle fracture in glassy materials			
R^2	a	b	c	d	e	ϵ_{rel}	a	b	c
PD [294]	0.83	0.99	0.98	0.98	0.78	PD [296]	$-0.21/-0.35$	$0/-0.12$	$-0.06/-0.06$
PF [293]	0.78	0.84	1	0.64	0.65	PF [296]	-0.51	0	-0.06
EXP [292]	-	-	-	-	-	EXP [295]	$57°/55°$	$\{0.53,0.57,0.88\}$Width	30.7 ± 1.5µs

5.1 Computational aspects

In this section, we focus on the computational aspects of both models from a bird's eye view and compare the computations on a very high-level. To do so, we define the quantity of a field which can be a vector field $\mathbf{f} = \{f_1, \ldots, f_n \,|\, f_i \in \mathbb{R}^3\}$ or a scalar field $f = \{f_1, \ldots, f_n \,|\, f_i \in \mathbb{R}\}$. For peridynamic, we have a so-called one-field model where one solves for the displacement field $\mathbf{u}$ and the peridynamic damage field $d(\mathbf{u})$ is evaluated using the displacement field. The displacement field is solved with explicit or implicit time integration [298–302]. However, the majority of PD simulations utilized bond-based models due to the increased computational costs for the state-based models. Similarly, the majority of simulations utilized explicit time integration due to their lower computational costs.

For phase-field, we have a two field models with the displacement field $\mathbf{u}$ and the damage field $\boldsymbol{\phi}$. For staggered schemes and alternating minimization [158, 216, 221, 222, 226–228, 303] the global system is decoupled, first, one solves for the displacement field $\mathbf{u}$ and second, one solves for the phase-field damage field $\boldsymbol{\phi}$ independently. For the equation of motion, implicit or explicit time integration schemes can be utilized. For the monolithic scheme [112, 172, 215, 230, 232, 233, 244, 304] the displacement field and the phase-field damage field are fully coupled and solved simultaneously. Pham et al. [119] suggested that a suitable choice of fracture process zone corresponding to the intrinsic length scale associated with the phase-field model could provide valid predictions of crack growth in quasi-static brittle fracture.

For calibrating the material models in most cases the same classical elasticity parameters can be utilized in both models. For the material properties, both models require a minimal set of parameters, *i.e.* Young's modulus E, Poisson's ratio ν, and fracture energy G_c, which all can be experimentally determined. Thus, both models could use the same elasticity properties obtained by an experiment to calibrate and validate against the same quantity of interest. Next to these parameters the length scale parameter l_0 for phase-field models and the horizon δ for peridynamic models needs to calibrated. Techniques for calibration that include material strength and flaw size have been shown for PF [305] and PD [25, 82]. On the other hand, when sharp cracks approximations are needed, mathematically l_0 should tend to zero (see Section 2.2), as confirmed for PF with numerical simulations in [237] using an academic test case in which manufactured solutions for the crack opening displacement and total crack volume were constructed [306]. In the case of PD with bond softening, one sees that the damage is confined to a thin zone about the crack line of thickness controlled by the PD horizon δ, [96]. Here the thickness is $\delta + 2h$ where the mesh diameter h is $h = o(\delta)$. Goswami et. al. [307] developed an enhanced physics-informed neural network (PINN) based machine learning (ML) for the fracture growth and propagation problem using PF. Nguyen et. al. [308] used ML to develop relationships between the displacements of a material point and the displacements of its neighbours and the applied forces within PD framework.

5.2 Advantages

Several advantages are highlighted for both PD and PF approaches to show why these two methods have been popular approaches to understand fracture phenomena.

1. **Crack initiation**: One unique selling point of both models is that there is no need of any initial crack, *e.g.* prescribed defects, in the model and cracks and fractures initiated over time. Another notable approach with the same feature is the eigen-erosion framework [309–312].

2. **Notion of damage in the model representation**: In most other models or computational techniques an additional criteria, *e.g.* as in Linear Elastic Fracture Mechanics, is needed to describe the growth of cracks. However, in peridynamic and phase-field models the criteria for the crack growth is determined as a part of the solution and no external criteria is needed.

3. **Increasing complexity in multi-field fracture**: Both models were extended to multi-field fracture. For peridynamic models: thermal effects [313–317], diffusion [80, 314, 318–320], geomechanical fracture [321–332], and corrosion [333–335]. For phase-field simulations: hydraulic fracture [125, 145–147, 276, 278, 336–339], diffusion [153], thermo-elastic-plastic [143], thermal effects [115, 141, 142, 214], and fluid-structure interaction [5, 270, 340].

5.3 Challenges

Following important issues are identified as challenges in the context of both PD and PF modeling:

Common challenges to PD and PF

1. **Computational cost**: Both PD and PF approaches are computationally expensive. For peridynamics it is the meshless discretization, which is computational intensive similar to molecular dynamics (MD) and smoothed-particle hydrodynamics (SPH). To accelerate the computations implementations using the Message Passing Interface (MPI) [53, 55, 56], the C++ standard library for parallelism and concurrency (HPX) [57], and GPU accelerated [60–62]

are available. To speed up the implicit time integration following methods were proposed: Finite element approaches (FEM) [49, 51, 54], a Galerkin method that exploits the matrix structure [341], using sparse matrices instead of a dense tangent stiffness matrix [342], adaptive dynamic relaxation schemes (ADR) [343–345], the Fire algorithm [346, 347], and the GMRES algorithm [348] in conjunction with the Arnoldi process [349, 350].

For phase-field models the length scale parameter l_0 tends to become small, thus, requiring small mesh sizes for finite element discretizations. Therefore, the method gets computationally expensive due to the large number of mesh elements. Phase-field models could be accelerated using a staggered schemes instead of a monolithic scheme [162], GPU acceleration [255], and the Message Passing Interface (MPI) based parallelization [173, 237], and matrix-free geometric multigrid methods [233, 238]. Other attempts to reduce the computational costs are model order reduction [351, 352], sympletic time integrators [353], adaptive schemes [146, 218, 221, 255, 257, 259, 260], and global/local (multiscale) approaches [240, 271, 273, 354].

2. **Lack of detailed three-dimensional simulations**: Probably due to their computational expenses, only a few three-dimensional simulations using PF and PD are reviewed here. Following three-dimensional PD simulations are available: hydraulic fracture [328, 355], the Brokenshire torsion experiment [356], polymer chains [357], Kalthoff Winkler [106], pitting corrosion damage [358], 3-point bending [63], impact damage on the glass layered structure [63, 359, 360], penny-shaped crack in a cylindrical bar [361], double edge notch specimen [361], ductile material behavior in a rectangular bar [362], pressurized cylinder [158], and reinforced concrete lap splice [27].

   The following three-dimensional research studies using PF are available: formation and growth of echelon cracks [164], pressure vessel simulation [158], single-edge notched shear test [162], cube with rigid spherical inclusion under tension [157], Kalthoff Winkler experiment [157], bolted plate compared against experimental results [161], simple shear tests of thoracic aorta with anisotropic failure compared against experimental results [163], random nucleation sites [159], L-shaped specimen [160, 233], tension test of cube with spherical inclusion [112], bending of Hopkinson bar [363], and Sneddon/Lowengrub benchmark [146, 217, 237], and non-isothermal pressurized fractures [364].

   To list some representative three-dimensional simulations, Weinberg et al. [365] showed stress distributions for modes I, II, and III fractures using NURBS-based finite elements in three-dimensional simulations. Heider et al. (2018) compared the hydraulic fracturing simulation results using PF against the experimental data for granite samples from the "Hohenberg" quarry in Germany with good predictive accuracy (within experimental relative errors less than 15%) for the pressure needed to initiate the crack in both 2D and 3D geometries. Another plausible reason for the lack of detailed three-dimensional fracture simulations could also be the associated challenges to perform detailed three-dimensional experimental measurements and provide validation data sets.

3. **Extraction of crack tip/surfaces**: Since both models have a notion of damage, the so-called phase-field crack function ϕ and the peridynamic damage parameter d, the position of the crack tip/surface is not encoded in the model and needs to be approximated. This phenomena is not limited to phase-field [207] and peridynamic models, *e.g.* [366, 367], and relates to any other method which does not have explicit crack representation in the model. This could be a source of error for tracking the crack tip and comparing the crack tip velocity against experimental observations in dynamic fracture simulations. Ziaei-Rad et al. (2016) used the non-maximum suppression technique from an image processing field to detect the ridge of the phase-field profile and then applied cubic spline fit to determine the crack path representation with reasonable success to identify crack branching as well as crack tips within the mesh resolution limits. Agrawal and Dayal [368] partially explained the relationship between phase-field and crack opening displacement and irreversibility in the phase-field model. Yoshioka et al. [369] presented two approaches - a line integral and a level-set method, to compute the crack opening displacement that is required in hydraulic fracturing simulations and demonstrated that both approaches computed the crack opening temporal growth accurately. Despite these recent advances, there is still room for improvement to extract the complex multiple interacting crack surfaces from simulations.

4. **Lack of validation studies against available experimental data**: Validation against exper-

imental data for peridynamics is summarized in [3] and for phase-field models in [4, Section 2.12]. However, for an accurate comparison of these two models, the same experiment or a set of experiments should be utilized to gain some insights of both methods on the same problem. Table 5 lists the phase-field and peridynamic models which were compared against the same experimental data. On the other hand, accessing raw experimental data is a different challenge [370], and one of the Sandia Fracture Challenges could be used to validate peridynamics and phase-field models against the same experimental data.

5. **Unavailability in the commercial codes**: Most simulations of PF and PD models use their implementations in corresponding scientific code bases. At the time of writing of this review, not many commercial codes implemented either one of the models. LS-DYNA provides a bond-based peridynamics implementation discretized with the discontinuous Galerkin FEM [63].

6. **Crack nucleation**: Despite crack nucleation being contained in both models, a final understanding from a theoretical point of view has not yet been fully achieved. However, simulations are available for PF [132, 305, 371] and PD [372–374].

7. **Incompressible hyper elastic material behavior**: At the time of completing this review, not many material models or simulations for incompressible hyper elastic material behavior, *e.g.* a Poisson ratio $\nu = 0.5$, were available for PF [208, 209] and PD [103, 375, 376]. Note that modeling of hyper elastic material behavior is challenging for any numerical method since the constitutive material law must reflect material behaviors such as a neo-Hookean [377] or Mooney–Rivlin [378] solids.

8. **Microscale view of crack propagation physics using molecular dynamics (MD) simulations**: Seleson et al. [97] showed that peridynamics (PD) model can recover the same dynamics as the MD model through appropriate selection of length scale for smooth deformations. Ahadi and Melin [379] investigated accuracy of PD in capturing features emerging from atomistic simulation [380] through calibration of interparticle bond strength and length scale parameters elastic plastic effects. In a similar attempt to connect the phase-field method to MD, Patil et al. [381] derived PFM parameters from the MD atomistic simulations and showed that the theoretical energy release rate G and internal length parameter are consistent with the MD simulation results. It is important to note that the microscale physics of crack nucleation and growth through MD atomistic simulation can provide the information for upscaling [382]. Given the current state of the art, the relation between first principles models and the macroscopic models of PD and PF with crack nucleation and propagation has not been firmly established in the literature.

Specific challenges for Peridynamics Fracture Model

The following challenges are highlighted to show the difficulties in applying boundary conditions, specific material models, and controlling numerical errors in PD.

1. **Application of boundary conditions:** As mentioned in [3] a major challenge within PD is the treatment of boundary conditions in a non-local fashion [383–387]. One approach is to couple local and non-local models to enforce boundary conditions in the local region and have the non-local model in the region where cracks and fractures arise. For more details we refer to the review on non-local coupling approaches [388].

2. **Constitutive modeling** Figure 2 illustrates the plethora of material models proposed for peridynamics. The question of choosing a nonlocal model that is an acceptable representative for a particular material system must be the focus of a coordinated theoretical and experimental effort.

3. **Choice of discretization parameters:** As mentioned in [3] the choice of the nodal spacing and the horizon results in diverse convergence scenarios [78, 81]. One challenge is to find the proper ratio between the horizon and mesh size, since the simulations are sensitive [82] with respect of these parameters. One adjustment is to select the ratio such that the PD simulation matches the dispersion curve obtained by the experiment [389]. Another adjustment is to determine the horizon by Griffith's brittle failure criterion [25]. To determine the discretization parameters from experimental data, the peridynamic formulation of the virtual field method could be applied [390].

4. **Ductile fracture**: As the time of writing this review, not many material models and simulation for ductile fracture were available [391–393]. Note that ductile tearing is challenging for any numerical method, due to the choice of an appropriate ductile failure model. This failure model needs to incorporate the failure of hydrostatic stress (or triaxiality of stress) to

predict ductile failure.

5. **Opportunities for quasistatic PD models:** The preponderance of peridynamic simulation has focused on dynamic problems and this provides an opportunity for quasistatic fracture modeling with suitable PD models. There are plenty of experimental benchmarks for the validation of peridynamic models in the quasistatic regime.

6. **Adaptive PD models and methods:** There is a lack of adaptive methods to handle peridynamic fracture problems. Nonlocal models are far more expensive than local models and can induce extra dispersive artifacts in otherwise local elastic regions this provides the motivation for adaptive local-nonlocal models for fracture evolution. Here the fracture set is evolved in terms of PD while FEM methods can be used away from the fracture set. To date, this type of numerical modeling has been implemented in [388].

7. **Asymptotically compatible quadrature methods:** Another way to control accuracy of peridynamic methods is through development of asymptotically compatible quadrature methods for fracture as in recent approach of [95]. Here the numerical scheme is designed to recover linear elastic behavior away from the crack set asymptotically as the horizon tends to zero.

Specific challenges for Phase-field Fracture Model

The following challenges are highlighted regarding the handling of complex geometries, material models, and controlling numerical errors in estimating crack surface geometries in PF.

1. **Crack path intersecting holes, obstacles, and boundaries**: Several issues were reported while obtaining crack paths in agreement with LEFM for problems involving holes [4]. Another study [120] concluded that judgement on if a crack arrests or the method simply does not permit continuation across obstacles, requires expert knowledge. In pressurized fractures, see e.g., [232], the fracture often branches, which raises however the question whether this is physically reasonable. Moreover, goal functional evaluations are sensitive to boundary conditions and the domain size [237].

2. **Fast crack propagation under dynamic loading**: For some fast crack propagation simulations, *e.g.* [368], the calculated fracture velocity overestimated the fracture energy dissipation.

3. **Composite/Concrete fracture**: At the time of writing this review, not many fracture/damage models for composites [194, 394, 395] and concrete [396–399] were available.

4. **Asymptotic computational understanding of the interaction of regularization, model, and discretization parameters**: In terms of numerical and computational convergence analysis, current PF understanding is still incomplete. Ingredients of numerical analysis from image segmentation [400], phase-field in fluid flow [401, 402] are available. Furthermore, computational convergences analyses for phase-field fracture have been undertaken [5, 218]. Such a rigorous numerical analysis for a phase-field fracture model substantiated with numerical tests is missing to date.

6 Conclusions

A comprehensive review of two numerical modeling approaches - Peridynamics (PD) and Phase-field (PF) is presented with the expectation to highlight their advantages, as well as challenges in modeling fracture initiation, propagation, and predictive capabilities for experimental validation. Both numerical methods can retrieve a consistent microscale physics of crack initiation and propagation. Despite both approaches being computationally challenging, their advantages in capturing multiple fracture interactions with minimal amount of phenomenological assumptions and closures make PD and PF as a good choice to understand engineering fracture mechanics. The following items are listed here for further improvement of both modeling approaches:

- Both PD and PF must be evaluated against the same experimental benchmark for a reasonable comparison in a blind validation manner. Several experimental datasets are identified as the available community resources.
- Phase-field simulation results for the Sandia fracture challenge problems could provide the missing piece of information for a comprehensive and validated comparison among the two modeling approaches.
- There is in general a lack of comparative studies between these two leading modeling approaches for fracture initiation and propagation even for the same set of simple fracture experiments.

Nomenclature

Peridynamic

δ	Peridynamic length scale parameter ($\delta \in \mathbb{R}^+$) [m]
$\mathbf{f}$	Pair-wise force function ($f : \mathbb{R}^n \times \mathbb{R}^n \times [0,T] \to \mathbb{R}^n$)
$\mathbf{X}$	Material point ($\mathbf{X} \in \mathbb{R}^n$)
μ	Peridynamic damage function $\mu : [0,T] \times \mathbb{R}^n \times \mathbb{R}^n \to \mathbb{R}$
$\underline{T}$	Peridynamic force state $T : \mathbb{R}^n \times \mathbb{R}^n \times [0,T] \to \mathbb{R}^n$
B_δ	Neighborhood of a PD material point $\mathbf{X}$
D	Peridynamic domain ($D \subset \mathbb{R}^n$)
d	Peridynamic damage variable $d : [0,T] \times \mathbb{R}^n \to \mathbb{R}$

Phase-field

Γ	Phase-field crack set ($\Gamma \subset \mathbb{R}^{n-1}$)
γ	Phase-field crack surface density function
$\mathbf{b}^*$	Phase-field body force [$\mathrm{N/m^3}$]
$\mathbf{t}^*$	Phase-field boundary traction [$\mathrm{Pa/m}$]
Ω	Phase-field domain ($\Omega \subset \mathbb{R}^n$)
$\partial\Omega$	Phase-field boundary ($\partial\Omega \subset \mathbb{R}^{n-1}$)
$\partial\Omega_t$	Phase-field traction boundary ($\partial\Omega_t \subset \mathbb{R}^{n-1}$)
$\partial\Omega_u$	Phase-field displacement boundary ($\partial\Omega_u \subset \mathbb{R}^{n-1}$)
ϕ	Phase-field crack function ($\phi \in [0,1]$)
ψ_c	Phase-field surface energy
ψ_s	Phase-field strain energy
l_0	Phase-field length scale parameter ($l_0 \in \mathbb{R}^+$) [m]
P	Phase-field external energy potential [J]

Other Symbols

$\ddot{\mathbf{u}}$	Acceleration ($\ddot{\mathbf{u}} \in \mathbb{R}^n$) [$\mathrm{m/s^2}$]
$\mathbf{u}$	Displacement ($\mathbf{u} \in \mathbb{R}^n$) [m]
ϱ	Material's density [$\mathrm{kg/m^3}$]
G_c	Critical energy release rate [$\mathrm{J\,m^{-2}}$]
n	Dimension $n = \{1,2,3\}$
T	Final Time [s]
t	Current time [s]

Disclaimer

The authors have made a diligent effort to cite all relevant work while avoiding the pitfalls of being exhaustive for the scope of this article. In case of inadvertent omission of any applicable citation, please accept our sincere apology. All authors declare no conflict of interest for this research.

Acknowledgments

This work was partly funded by DTIC Contract FA8075-14-D-0002/0007 and the Center of Computation & Technology at Louisiana State University. Authors also thank Dr. Stewart Silling for his comments on the manuscript prior to the submission and the participants of the Workshop on Experimental and Computational Fracture Mechanics[12] and of the Banff International Research Station: Hydraulic Fracturing: Modeling, Simulation, and Experiment[13] for the discussion on peridynamics and phase-field models which provided several ideas for the challenging applications. This material is partially based upon work supported by the U. S. Army Research Laboratory and the U. S. Army Research Office under Contract/Grant Number W911NF1610456. TW was partially funded by the the German Research Foundation, Priority Program 1748 (DFG SPP 1748) under the grant number WI4367/2-1 and project number 392587580.

References

[1] Silling, S., Wick, T., Ravi-Chandar, K., Guilleminot, J., Dolbow, J., Finberg, J., Diehl, P., Prudhomme, S., Lipton, R., and Seleson, P., 2020. Workshop on experimental and computational fracture mechanics 2020. Tech. Rep. ORNL/TM-2020/1714, Oak Ridge National Laboratory, Nov.

[2] Javili, A., Morasata, R., Oterkus, E., and Oterkus, S., 2019. "Peridynamics review". *Mathematics and Mechanics of Solids,* **24**(11), pp. 3714–3739.

[3] Diehl, P., Prudhomme, S., and Lévesque, M., 2019. "A review of benchmark experiments for the validation of peridynamics models". *Journal of Peridynamics and Nonlocal Modeling,* **1**(1), pp. 14–35.

[4] Wu, J.-Y., Nguyen, V. P., Thanh Nguyen, C., Sutula, D., Bordas, S., and Sinaie, S., 2019. "Phase field modelling of fracture". *Advances in Applied Mechanics,* **53**, 09.

[5] Wick, T., 2020. *Multiphysics Phase-Field Fracture: Modeling, Adaptive Discretizations, and Solvers*. De Gruyter, Berlin, Boston.

[6] Cucker, F., and Smale, S., 2007. "Emergent behavior in flocks". *Trans. Autom. Control,* **52**, pp. 852–862.

[7] Trygve K. Karper, A. M., and Trivisa, K., 2015. "Hydrodynamic limit of the kinetic cucker–smale flocking model". *Mathematical Models and methods in the Applied Sciences M3AS,* **25**, pp. 131–163.

[8] Figalli, A., and Kang, M.-J., 2019. "A rigorous derivation from the kinetic cucker–smale model to

[12] Playlist (WFM2020)

[13] Playlist (Hydraulic Fracturing: Modeling, Simulation, and Experiment)

the pressureless euler system with nonlocal alignment". *Analysis & PDE,* **12**(3), pp. 843 – 866.

[9] Tadmor, R. S. . E., 2020. "Flocking hydrodynamics with external potentials". *Archive for Rational Mechanics and Analysis,* **238**, pp. 347–1381.

[10] Silling, S., 2000. "Reformulation of elasticity theory for discontinuities and long-range forces". *Journal of the Mechanics and Physics of Solids,* **48**(1), pp. 175–209.

[11] Silling, S. A., and Askari, E., 2005. "A meshfree method based on the peridynamic model of solid mechanics". *Computers & structures,* **83**(17-18), pp. 1526–1535.

[12] Kunin, I. A., 2012. *Elastic media with microstructure I: one-dimensional models*, Vol. 26. Springer Science & Business Media.

[13] Kunin, I. A., 2012. *Elastic Media with Microstructure II: Three-Dimensional Models (Springer Series in Solid-State Sciences)*, softcover reprint of the original 1st ed. 1983 ed. Springer, 1.

[14] Silling, S. A., Epton, M., Weckner, O., Xu, J., and Askari, E., 2007. "Peridynamic states and constitutive modeling". *Journal of Elasticity,* **88**(2), pp. 151–184.

[15] Foster, J. T., Silling, S. A., and Chen, W., 2011. "An energy based failure criterion for use with peridynamic states". *International Journal for Multiscale Computational Engineering,* **9**(6).

[16] Zhang, Y., and Qiao, P., 2019. "A new bond failure criterion for ordinary state-based peridynamic mode ii fracture analysis". *International Journal of Fracture,* **215**(1-2), pp. 105–128.

[17] Dipasquale, D., Shojaei, A., and Yooyen, S., 2020. "A novel stress tensor-based failure criterion for peridynamics". In Multidisciplinary Digital Publishing Institute Proceedings, Vol. 39, p. 23.

[18] Madenci, E., and Oterkus, E., 2014. *Peridynamic Theory*. Springer.

[19] Bobaru, F., Foster, J. T., Geubelle, P. H., and Silling, S. A., 2016. *Handbook of peridynamic modeling*. CRC press.

[20] Ganzenmueller, G., Hiermaier, S., and May, M., 2013. "Improvements to the prototype micro-brittle linear elasticity model of peridynamics". *Lecture Notes in Computational Science and Engineering,* **100**, 12.

[21] Hu, W., Ha, Y. D., and Bobaru, F., 2011. "Modeling dynamic fracture and damage in a fiber-reinforced composite lamina with peridynamics". *International Journal for Multiscale Computational Engineering,* **9**(6).

[22] Hu, W., Ha, Y. D., and Bobaru, F., 2012. "Peridynamic model for dynamic fracture in unidirectional fiber-reinforced composites". *Computer Methods in Applied Mechanics and Engineering,* **217-220**, pp. 247–261.

[23] Kilic, B., and Madenci, E., 2009. "Prediction of crack paths in a quenched glass plate by using peridynamic theory". *International Journal of Fracture,* **156**(2), Apr, pp. 165–177.

[24] Kilic, B., 2008. *Peridynamic Theory for Progressive Failure Prediction in Homogeneous and Heterogeneous Materials*. The University of Arizona.

[25] Diehl, P., Lipton, R., and Schweitzer, M., 2016. "Numerical verification of a bond-based softening peridynamic model for small displacements: deducing material parameters from classical linear theory". *Institut für Numerische Simulation Preprint*(1630).

[26] Lipton, R., 2016. "Cohesive dynamics and brittle fracture". *Journal of Elasticity,* **124**(2), pp. 143–191.

[27] Gerstle, W., Sakhavand, N., and Chapman, S., 2010. "Peridynamic and continuum models of reinforced concrete lap splice compared". *Fracture Mechanics of Concrete and Concrete Structures-Recent Advances in Fracture Mechanics of Concrete*.

[28] Aziz, A., 2014. "Simulation of fracture of concrete using micropolar peridynamics". PhD thesis, The University of New Mexico.

[29] Silling, S. A., 2019. "Attenuation of waves in a viscoelastic peridynamic medium". *Mathematics and Mechanics of Solids,* **24**(11), pp. 3597–3613.

[30] Hu, Y., and Madenci, E., 2017. "Peridynamics for fatigue life and residual strength prediction of composite laminates". *Composite Structures,* **160**, pp. 169–184.

[31] Askari, E., Xu, J., and Silling, S., 2006. "Peridynamic analysis of damage and failure in composites". In 44th AIAA aerospace sciences meeting and exhibit, p. 88.

[32] Hu, Y., De Carvalho, N., and Madenci, E., 2015. "Peridynamic modeling of delamination growth in composite laminates". *Composite Structures,* **132**, pp. 610–620.

[33] Zhang, T., and Zhou, X., 2019. "A modified axisymmetric ordinary state-based peridynamics with shear deformation for elastic and fracture problems in brittle solids". *European Journal of Mechanics - A/Solids,* **77**, p. 103810.

[34] Lai, X., Liu, L., Zeleke, M., Liu, Q., and Wang, Z., 2018. "A non-ordinary state-based peridynamics modeling of fractures in quasi-brittle materials". *International Journal of Impact Engineering,* **111**, 01.

[35] Gao, Y., and Oterkus, S., 2019. "Ordinary state-based peridynamic modelling for fully coupled

thermoelastic problems". *Continuum Mechanics and Thermodynamics,* **31**(4), pp. 907–937.

[36] Rahaman, M. M., Roy, P., Roy, D., and Reddy, J., 2017. "A peridynamic model for plasticity: Micro-inertia based flow rule, entropy equivalence and localization residuals". *Computer Methods in Applied Mechanics and Engineering,* **327**, pp. 369–391. Advances in Computational Mechanics and Scientific Computation—the Cutting Edge.

[37] Kružík, M., Mora-Corral, C., and Stefanelli, U., 2018. "Quasistatic elastoplasticity via peridynamics: existence and localization". *Continuum Mechanics and Thermodynamics,* **30**(5), Sep, pp. 1155–1184.

[38] Madenci, E., and Oterkus, S., 2016. "Ordinary state-based peridynamics for plastic deformation according to von mises yield criteria with isotropic hardening". *Journal of the Mechanics and Physics of Solids,* **86**, pp. 192–219.

[39] Oterkus, E., 2010. "Peridynamic theory for modeling three-dimensional damage growth in metallic and composite structures". PhD thesis, The University of Arizona.

[40] Silling, S. A., Parks, M. L., Kamm, J. R., Weckner, O., and Rassaian, M., 2017. "Modeling shock-waves and impact phenomena with eulerian peridynamics". *International Journal of Impact Engineering,* **107**, pp. 47–57.

[41] Mitchell, J., Silling, S., and Littlewood, D., 2015. "A position-aware linear solid constitutive model for peridynamics". *Journal of Mechanics of Materials and Structures,* **10**(5), pp. 539–557.

[42] Weckner, O., and Mohamed, N. A. N., 2013. "Viscoelastic material models in peridynamics". *Applied Mathematics and Computation,* **219**(11), pp. 6039–6043.

[43] Mitchell, J. A., 2011. "A non-local, ordinary-state-basedviscoelasticity model forperidynamics". *SANDIA REPORT,* **SAND2011-8064**, October.

[44] Delorme, R., Tabiai, I., Laberge Lebel, L., and Lévesque, M., 2017. "Generalization of the ordinary state-based peridynamic model for isotropic linear viscoelasticity". *Mechanics of Time-Dependent Materials,* **21**(4), Nov, pp. 549–575.

[45] Madenci, E., and Oterkus, S., 2017. "Ordinary state-based peridynamics for thermoviscoelastic deformation". *Engineering Fracture Mechanics,* **175**, pp. 31–45.

[46] Tupek, M., and Radovitzky, R., 2014. "An extended constitutive correspondence formulation of peridynamics based on nonlinear bond-strain measures". *Journal of the Mechanics and Physics of Solids,* **65**, pp. 82–92.

[47] O'Grady, J., and Foster, J., 2014. "Peridynamic plates and flat shells: A non-ordinary, state-based model". *International Journal of Solids and Structures,* **51**(25), pp. 4572–4579.

[48] Yaghoobi, A., Chorzepa, M., Kim, S., et al., 2017. "Mesoscale fracture analysis of multiphase cementitious composites using peridynamics". *Materials,* **10**(2), p. 162.

[49] Chen, X., and Gunzburger, M., 2011. "Continuous and discontinuous finite element methods for a peridynamics model of mechanics". *Computer Methods in Applied Mechanics and Engineering,* **200**(9-12), pp. 1237–1250.

[50] Jha, P. K., and Lipton, R., 2020. "Finite element convergence for state-based peridynamic fracture models". *Communications on Applied Mathematics and Computation,* **2**(1), Aug, pp. 93–128.

[51] Macek, R. W., and Silling, S. A., 2007. "Peridynamics via finite element analysis". *Finite Elements in Analysis and Design,* **43**(15), pp. 1169–1178.

[52] Weckner, O., and Emmrich, E., 2005. "Numerical simulation of the dynamics of a nonlocal, inhomogeneous, infinite bar". *J. Comput. Appl. Mech,* **6**(2), pp. 311–319.

[53] Parks, M. L., Lehoucq, R. B., Plimpton, S. J., and Silling, S. A., 2008. "Implementing peridynamics within a molecular dynamics code". *Computer Physics Communications,* **179**(11), pp. 777–783.

[54] Emmrich, E., and Weckner, O., 2007. "The peridynamic equation and its spatial discretisation". *Mathematical Modelling and Analysis,* **12**(1), pp. 17–27.

[55] Littlewood, D. J., 2015. Roadmap for peridynamic software implementation. Tech. Rep. 2015-9013, Sandia National Laboratories.

[56] Parks, M., Littlewood, D., Mitchell, J., and Silling, S., 2012. Peridigm users' guide. Tech. Rep. SAND2012-7800, Sandia National Laboratories.

[57] Diehl, P., Jha, P. K., Kaiser, H., Lipton, R., and Lévesque, M., 2020. "An asynchronous and task-based implementation of peridynamics utilizing hpx—the c++ standard library for parallelism and concurrency". *SN Applied Sciences,* **2**(12), Dec, p. 2144.

[58] Heller, T., Diehl, P., Byerly, Z., Biddiscombe, J., and Kaiser, H., 2017. "Hpx–an open source c++ standard library for parallelism and concurrency". *Proceedings of OpenSuCo*, p. 5.

[59] Kaiser, H., Diehl, P., Lemoine, A. S., Lelbach, B. A., Amini, P., Berge, A., Biddiscombe, J., Brandt, S. R., Gupta, N., Heller, T., Huck, K., Khatami, Z., Kheirkhahan, A., Reverdell, A., Shirzad, S., Simberg, M., Wagle, B., Wei, W., and Zhang, T., 2020. "Hpx - the c++ standard library

for parallelism and concurrency". *Journal of Open Source Software,* **5**(53), p. 2352.

[60] Mossaiby, F., Shojaei, A., Zaccariotto, M., and Galvanetto, U., 2017. "Opencl implementation of a high performance 3d peridynamic model on graphics accelerators". *Computers & Mathematics with Applications,* **74**(8), pp. 1856–1870.

[61] Diehl, P., 2012. "Implementierung eines Peridynamik-Verfahrens auf GPU". Diplomarbeit, Institute of Parallel and Distributed Systems, University of Stuttgart.

[62] Diehl, P., and Schweitzer, M. A., 2015. "Efficient neighbor search for particle methods on gpus". In *Meshfree Methods for Partial Differential Equations VII*. Springer, pp. 81–95.

[63] Ren, B., Wu, C., and Askari, E., 2017. "A 3d discontinuous galerkin finite element method with the bond-based peridynamics model for dynamic brittle failure analysis". *International Journal of Impact Engineering,* **99**, pp. 14–25.

[64] Silling, S., 2001. "Peridynamic modeling of the kalthoff–winkler experiment". *Submission for the*.

[65] Emmrich, E., Weckner, O., et al., 2007. "On the well-posedness of the linear peridynamic model and its convergence towards the navier equation of linear elasticity". *Communications in Mathematical Sciences,* **5**(4), pp. 851–864.

[66] Du, Q., and Zhou, K., 2011. "Mathematical analysis for the peridynamic nonlocal continuum theory". *ESAIM: Mathematical Modelling and Numerical Analysis,* **45**(2), pp. 217–234.

[67] Erbay, H. A., Erkip, A., and Muslu, G. M., 2012. "The cauchy problem for a one-dimensional nonlinear elastic peridynamic model". *Journal of Differential Equations,* **252**(8), pp. 4392–4409.

[68] Du, Q., Kamm, J. R., Lehoucq, R. B., and Parks, M. L., 2012. "A new approach for a nonlocal, nonlinear conservation law". *SIAM Journal on Applied Mathematics,* **72**(1), pp. 464–487.

[69] Emmrich, E., and Puhst, D., 2013. "Well-posedness of the peridynamic model with lipschitz continuous pairwise force function". *Communications in Mathematical Sciences,* **11**(4), pp. 1039–1049.

[70] Bellido, J. C., and Mora-Corral, C., 2014. "Existence for nonlocal variational problems in peridynamics". *SIAM Journal on Mathematical Analysis,* **46**(1), pp. 890–916.

[71] Mengesha, T., and Du, Q., 2015. "On the variational limit of a class of nonlocal functionals related to peridynamics". *Nonlinearity,* **28**(11), p. 3999.

[72] Aksoylu, B., and Parks, M. L., 2011. "Variational theory and domain decomposition for nonlocal problems". *Applied Mathematics and Computation,* **217**(14), pp. 6498–6515.

[73] Du, Q., Gunzburger, M., Lehoucq, R. B., and Zhou, K., 2012. "Analysis and approximation of nonlocal diffusion problems with volume constraints". *SIAM review,* **54**(4), pp. 667–696.

[74] Du, Q., Gunzburger, M., Lehoucq, R., and Zhou, K., 2013. "Analysis of the volume-constrained peridynamic navier equation of linear elasticity". *Journal of Elasticity,* **113**(2), pp. 193–217.

[75] Du, Q., Gunzburger, M., Lehoucq, R. B., and Zhou, K., 2013. "A nonlocal vector calculus, nonlocal volume-constrained problems, and nonlocal balance laws". *Mathematical Models and Methods in Applied Sciences,* **23**(03), pp. 493–540.

[76] Seleson, P., Du, Q., and Parks, M. L., 2016. "On the consistency between nearest-neighbor peridynamic discretizations and discretized classical elasticity models". *Computer Methods in Applied Mechanics and Engineering,* **311**, pp. 698–722.

[77] Ganzenmüller, G. C., Hiermaier, S., and May, M., 2015. "On the similarity of meshless discretizations of peridynamics and smooth-particle hydrodynamics". *Computers & Structures,* **150**, pp. 71–78.

[78] Du, Q., and Tian, X., 2015. "Robust discretization of nonlocal models related to peridynamics". In *Meshfree methods for partial differential equations VII*. Springer, pp. 97–113.

[79] Zhou, K., and Du, Q., 2010. "Mathematical and numerical analysis of linear peridynamic models with nonlocal boundary conditions". *SIAM Journal on Numerical Analysis,* **48**(5), pp. 1759–1780.

[80] Tian, X., and Du, Q., 2013. "Analysis and comparison of different approximations to nonlocal diffusion and linear peridynamic equations". *SIAM Journal on Numerical Analysis,* **51**(6), pp. 3458–3482.

[81] Tian, X., and Du, Q., 2014. "Asymptotically compatible schemes and applications to robust discretization of nonlocal models". *SIAM Journal on Numerical Analysis,* **52**(4), pp. 1641–1665.

[82] Diehl, P., Franzelin, F., Pflüger, D., and Ganzenmüller, G. C., 2016. "Bond-based peridynamics: a quantitative study of mode i crack opening". *International Journal of Fracture,* **201**(2), pp. 157–170.

[83] Franzelin, F., Diehl, P., and Pflüger, D., 2015. "Non-intrusive uncertainty quantification with sparse grids for multivariate peridynamic simulations". In *Meshfree Methods for Partial Differential Equations VII*. Springer, pp. 115–143.

[84] Lipton, R., 2014. "Dynamic brittle fracture as a small horizon limit of peridynamics". *Journal of Elasticity,* **117**, pp. 21–50.

[85] Jha, P. K., and Lipton, R., 2018. *Well-Posed Nonlinear Nonlocal Fracture Models Associated with Double-Well Potentials*. Springer International Publishing, pp. 1–40.

[86] Puhst, E. E. . D., 2016. "A short note on modelling damage in peridynamics". *Journal of Elasticity,* **123**, pp. 245–252.

[87] Du, Q., Tao, Y., and Tian, X., 2017. "A peridynamic model of fracture mechanics with bond-breaking". *Journal of Elasticity,* **132**, pp. 197–218.

[88] Lipton, R., Said, E., and Jha, P., 2018. "Free damage propagation with memory". *Journal of Elasticity,* **133**(2), pp. 129–153.

[89] Jha, P. K., and Lipton, R., 2018. "Numerical analysis of nonlocal fracture models in holder space". *SIAM Journal on Numerical Analysis,* **56**(2), pp. 906–941.

[90] Jha, P. K., and Lipton, R., 2019. "Numerical convergence of finite difference approximations for state based peridynamic fracture models". *Computer Methods in Applied Mechanics and Engineering,* **351**, pp. 184–225.

[91] Jha, P. K., and Lipton, R., 2021. "Finite element approximation of nonlocal dynamic fracture models". *Discrete & Continuous Dynamical Systems - B,* **26**(3), pp. 1675–1710.

[92] Lipton, R. P., Lehoucq, R. B., and Jha, P. K., 2019. "Complex fracture nucleation and evolution with nonlocal elastodynamics". *Journal of Peridynamics and Nonlocal Modeling,* **1**(2), pp. 122–130.

[93] Lipton, R. P., and Jha, P. K., 2021. "Nonlocal elastodynamics and fracture". *Nonlinear Differential Equations and Applications*(Published online.).

[94] DalMaso, G., and Toader, R., 2019. "On the cauchy problem for the wave equation on time-dependent domains". *Journal of Differential Equations,* **266**(6), pp. 3209–3246.

[95] Trask, N., You, H., Yu, Y., and Parks, M. L., 2007. "An asymptotically compatible meshfree quadrature rule for nonlocal problems with applications to peridynamics". *Computer Methods in Applied Mechanics and Engineering,* **343**, pp. 151–165.

[96] Jha, P. K., and Lipton, R., 2020. "Kinetic relations and local energy balance for LEFM from a nonlocal peridynamic model". *International Journal of Fracture,* **226**(1), pp. 81–95.

[97] Seleson, P., Parks, M. L., Gunzburger, M., and Lehoucq, R. B., 2009. "Peridynamics as an upscaling of molecular dynamics". *Multiscale Modeling & Simulation,* **8**(1), pp. 204–227.

[98] Diehl, P., 2017. "Modeling and simulation of cracks and fractures with peridynamics in brittle materials". PhD thesis, University of Bonn, Germany.

[99] Ahrens, J., Geveci, B., and Law, C., 2005. "Paraview: An end-user tool for large data visualization". *The visualization handbook,* **717**.

[100] Childs, H., Brugger, E., Whitlock, B., Meredith, J., Ahern, S., Pugmire, D., Biagas, K., Miller, M., Harrison, C., Weber, G. H., Krishnan, H., Fogal, T., Sanderson, A., Garth, C., Bethel, E. W., Camp, D., Rübel, O., Durant, M., Favre, J. M., and Navrátil, P., 2012. "VisIt: An End-User Tool For Visualizing and Analyzing Very Large Data". In *High Performance Visualization–Enabling Extreme-Scale Scientific Insight*. Oct, pp. 357–372.

[101] Levine, J. A., Bargteil, A. W., Corsi, C., Tessendorf, J., and Geist, R., 2014. "A peridynamic perspective on spring-mass fracture". In Proceedings of the ACM SIGGRAPH/Eurographics Symposium on Computer Animation, Eurographics Association, pp. 47–55.

[102] Chen, W., Zhu, F., Zhao, J., Li, S., and Wang, G., 2018. "Peridynamics-based fracture animation for elastoplastic solids". In Computer Graphics Forum, Vol. 37, Wiley Online Library, pp. 112–124.

[103] Xu, L., He, X., Chen, W., Li, S., and Wang, G., 2018. "Reformulating hyperelastic materials with peridynamic modeling". In Computer Graphics Forum, Vol. 37, Wiley Online Library, pp. 121–130.

[104] Diehl, P., Bußler, M., Pflüger, D., Frey, S., Ertl, T., Sadlo, F., and Schweitzer, M. A., 2017. "Extraction of fragments and waves after impact damage in particle-based simulations". In *Meshfree Methods for Partial Differential Equations VIII*. Springer, pp. 17–34.

[105] Littlewood, D., Silling, S., and Demmie, P., 2016. "Identification of fragments in a meshfree peridynamic simulation". In ASME 2016 International Mechanical Engineering Congress and Exposition, American Society of Mechanical Engineers, pp. V009T12A071–V009T12A071.

[106] Bussler, M., Diehl, P., Pflüger, D., Frey, S., Sadlo, F., Ertl, T., and Schweitzer, M. A., 2017. "Visualization of fracture progression in peridynamics". *Computers & Graphics,* **67**, pp. 45–57.

[107] Francfort, G., and Marigo, J.-J., 1998. "Revisiting brittle fracture as an energy minimization problem". *Journal of the Mechanics and Physics of Solids,* **46**(8), pp. 1319–1342.

[108] Aranson, I., Kalatsky, V., and Vinokur, V., 2000. "Continuum field description of crack propagation". *Physical review letters,* **85**(1), p. 118.

[109] Bourdin, B., Francfort, G. A., and Marigo, J.-J., 2000. "Numerical experiments in revisited brittle fracture". *Journal of the Mechanics and Physics of Solids,* **48**(4), pp. 797–826.

[110] Bourdin, B., Francfort, G., and Marigo, J.-J., 2008. "The variational approach to fracture". *J. Elasticity,* **91**(1-3), pp. 1–148.

[111] Bourdin, B., and Francfort, G. A., 2019. "Past and present of variational fracture". *SIAM News,* **52**(9).

[112] Miehe, C., Welschinger, F., and Hofacker, M., 2010. "Thermodynamically consistent phase-field models of fracture: Variational principles and multi-field fe implementations". *International Journal for Numerical Methods in Engineering,* **83**(10), pp. 1273–1311.

[113] Ambrosio, L., and Tortorelli, V., 1990. "Approximation of functionals depending on jumps by elliptic functionals via γ-convergence". *Comm. Pure Appl. Math.,* **43**, pp. 999–1036.

[114] Ambrosio, L., and Tortorelli, V., 1992. "On the approximation of free discontinuity problems". *Boll. Un. Mat. Ital. B,* **6**, pp. 105–123.

[115] Bourdin, B., Marigo, J.-J., Maurini, C., and Sicsic, P., 2014. "Morphogenesis and propagation of complex cracks induced by thermal shocks". *Physical review letters,* **112**(1), p. 014301.

[116] Wu, J.-Y., 2017. "A unified phase-field theory for the mechanics of damage and quasi-brittle failure". *Journal of the Mechanics and Physics of Solids,* **103**, pp. 72–99.

[117] Sargado, J. M., Keilegavlen, E., Berre, I., and Nordbotten, J. M., 2018. "High-accuracy phase-field models for brittle fracture based on a new family of degradation functions". *Journal of the Mechanics and Physics of Solids,* **111**, pp. 458–489.

[118] Braides, A., 1998. *Approximation of free-discontinuity problems*. Springer Science & Business Media.

[119] Pham, K., Ravi-Chandar, K., and Landis, C., 2017. "Experimental validation of a phase-field model for fracture". *International Journal of Fracture,* **205**(1), pp. 83–101.

[120] Egger, A., Pillai, U., Agathos, K., Kakouris, E., Chatzi, E., Aschroft, I. A., and Triantafyllou, S. P., 2019. "Discrete and phase field methods for linear elastic fracture mechanics: a comparative study and state-of-the-art review". *Applied Sciences,* **9**(12), p. 2436.

[121] Neitzel, I., Wick, T., and Wollner, W., 2017. "An optimal control problem governed by a regularized phase-field fracture propagation model". *SIAM Journal on Control and Optimization,* **55**(4), pp. 2271–2288.

[122] Mikelić, A., Wheeler, M. F., and Wick, T., 2015. "A quasi-static phase-field approach to pressurized fractures". *Nonlinearity,* **28**(5), pp. 1371–1399.

[123] Osher, S., and Sethian, J., 1988. "Fronts propagating with curvature-dependent speed: algorithms based on Hamiltonian-Jacobi formulations". *J. Comput. Phys.,* **79**(1), pp. 12–49.

[124] Lee, S., Wheeler, M. F., and Wick, T., 2017. "Iterative coupling of flow, geomechanics and adaptive phase-field fracture including level-set crack width approaches". *Journal of Computational and Applied Mathematics,* **314**, pp. 40 – 60.

[125] Wheeler, M. F., Wick, T., and Lee, S., 2020. "IPACS: Integrated Phase-Field Advanced Crack Propagation Simulator. An adaptive, parallel, physics-based-discretization phase-field framework for fracture propagation in porous media". *Computer Methods in Applied Mechanics and Engineering,* **367**, p. 113124.

[126] dal Maso, G., and Toader, R., 2002. "A model for the quasistatic growth of brittle fractures: existence and approximation results". *Arch. Ration. Mech. Anal.,* **162**, pp. 101–135.

[127] Francfort, G. A., and Larsen, C. J., 2003. "Existence and convergence for quasi-static evolution in brittle fracture". *Communications on Pure and Applied Mathematics,* **56**(10), pp. 1465–1500.

[128] dal Maso, G., Francfort, G. A., and Toader, R., 2005. "Quasistatic crack growth in nonlinear elasticity". *Arch. Ration. Mech. Anal.,* **176**, pp. 165–225.

[129] Larsen, C. J., Ortner, C., and Süli, E., 2010. "Existence of solutions to a regularized model of dynamics fracture". *Methods in Applied Sciences,* **20**, pp. 1021–1048.

[130] Chambolle, A., Giacomini, A., and Ponsiglione, M., 2008. "Crack initiation in brittle materials". *Arch. Ration. Mech. Anal.,* **188**, pp. 309–349.

[131] van Goethem, N., and Novotny, A., 2010. "Crack nucleation sensitivity analysis". *Math. Methods Appl. Sci.,* **33**(16).

[132] Kumar, A., Bourdin, B., Francfort, G. A., and Lopez-Pamies, O., 2020. "Revisiting nucleation in the phase-field approach to brittle fracture". *Journal of the Mechanics and Physics of Solids,* **142**, p. 104027.

[133] Chambolle, A., Francfort, G., and Marigo, J.-J., 2009. "When and how do cracks propagate?". *Journal of the Mechanics and Physics of Solids,* **57**(9), pp. 1614–1622.

[134] Larsen, C. J., Ortner, C., and Süli, E., 2010. "Existence of solutions to a regularized model of dynamic fracture". *Mathematical Models and Methods in Applied Sciences,* **20**(07), pp. 1021–1048.

[135] Francfort, G., 2021. "Variational fracture: twenty years after". *International Journal of Fracture*, pp. 1–11.

[136] Caputo, M., and Fabrizio, M., 2015. "Damage and fatigue described by a fractional derivative model". *Journal of Computational Physics,* **293**, pp. 400–408.

[137] Amendola, G., Fabrizio, M., and Golden, J., 2016. "Thermomechanics of damage and fatigue by a

phase field model". *Journal of Thermal Stresses,* **39**(5), pp. 487–499.

[138] Boldrini, J., de Moraes, E. B., Chiarelli, L., Fumes, F., and Bittencourt, M., 2016. "A non-isothermal thermodynamically consistent phase field framework for structural damage and fatigue". *Computer Methods in Applied Mechanics and Engineering,* **312**, pp. 395–427.

[139] Alessi, R., Vidoli, S., and De Lorenzis, L., 2018. "A phenomenological approach to fatigue with a variational phase-field model: The one-dimensional case". *Engineering Fracture Mechanics,* **190**, pp. 53–73.

[140] Seiler, M., Hantschke, P., Brosius, A., and Kästner, M., 2018. "A numerically efficient phase-field model for fatigue fracture–1d analysis". *PAMM,* **18**(1), p. e201800207.

[141] Miehe, C., Schaenzel, L.-M., and Ulmer, H., 2015. "Phase field modeling of fracture in multi-physics problems. part i. balance of crack surface and failure criteria for brittle crack propagation in thermo-elastic solids". *Computer Methods in Applied Mechanics and Engineering,* **294**, pp. 449–485.

[142] Schlüter, A., Kuhn, C., and Müller, R., 2017. "Simulation of laser-induced controlled fracturing utilizing a phase field model". *Journal of Computing and Information Science in Engineering,* **17**(2), p. 021001.

[143] Miehe, C., Hofacker, M., Schänzel, L.-M., and Aldakheel, F., 2015. "Phase field modeling of fracture in multi-physics problems. part ii. coupled brittle-to-ductile failure criteria and crack propagation in thermo-elastic–plastic solids". *Computer Methods in Applied Mechanics and Engineering,* **294**, pp. 486–522.

[144] Radszuweit, M., and Kraus, C., 2017. "Modeling and simulation of non-isothermal rate-dependent damage processes in inhomogeneous materials using the phase-field approach". *Computational Mechanics,* **60**(1), pp. 163–179.

[145] Mikelic, A., Wheeler, M. F., and Wick, T., 2015. "A phase-field method for propagating fluid-filled fractures coupled to a surrounding porous medium". *Multiscale Modeling & Simulation,* **13**(1), pp. 367–398.

[146] Lee, S., Wheeler, M. F., and Wick, T., 2016. "Pressure and fluid-driven fracture propagation in porous media using an adaptive finite element phase field model". *Computer Methods in Applied Mechanics and Engineering,* **305**, pp. 111–132.

[147] Zhou, S., Zhuang, X., and Rabczuk, T., 2018. "A phase-field modeling approach of fracture propagation in poroelastic media". *Engineering Geology,* **240**, pp. 189–203.

[148] Shanthraj, P., Svendsen, B., Sharma, L., Roters, F., and Raabe, D., 2017. "Elasto-viscoplastic phase field modelling of anisotropic cleavage fracture". *Journal of the Mechanics and Physics of Solids,* **99**, pp. 19–34.

[149] Diehl, M., Wicke, M., Shanthraj, P., Roters, F., Brueckner-Foit, A., and Raabe, D., 2017. "Coupled crystal plasticity–phase field fracture simulation study on damage evolution around a void: pore shape versus crystallographic orientation". *JOM,* **69**(5), pp. 872–878.

[150] Duda, F. P., Ciarbonetti, A., Toro, S., and Huespe, A. E., 2018. "A phase-field model for solute-assisted brittle fracture in elastic-plastic solids". *International Journal of Plasticity,* **102**, pp. 16–40.

[151] Nguyen, T.-T., Bolivar, J., Réthoré, J., Baietto, M.-C., and Fregonese, M., 2017. "A phase field method for modeling stress corrosion crack propagation in a nickel base alloy". *International Journal of Solids and Structures,* **112**, pp. 65–82.

[152] Martínez-Pañeda, E., Golahmar, A., and Niordson, C. F., 2018. "A phase field formulation for hydrogen assisted cracking". *Computer Methods in Applied Mechanics and Engineering,* **342**, pp. 742–761.

[153] Wu, T., and De Lorenzis, L., 2016. "A phase-field approach to fracture coupled with diffusion". *Computer Methods in Applied Mechanics and Engineering,* **312**, pp. 196–223.

[154] Klinsmann, M., Rosato, D., Kamlah, M., and McMeeking, R. M., 2016. "Modeling crack growth during li insertion in storage particles using a fracture phase field approach". *Journal of the Mechanics and Physics of Solids,* **92**, pp. 313–344.

[155] Roubicek, T., and Vodicka, R., 2019. "A monolithic model for phase-field fracture and waves in solid–fluid media towards earthquakes". *International Journal of Fracture,* **219**(1), Aug, p. 135–152.

[156] Kruzik, M., and Roubicek, T., 2019. *Mathematical methods in continuum mechanics of solids*. Springer.

[157] Hofacker, M., and Miehe, C., 2012. "Continuum phase field modeling of dynamic fracture: variational principles and staggered fe implementation". *International Journal of Fracture,* **178**(1-2), pp. 113–129.

[158] Borden, M. J., Verhoosel, C. V., Scott, M. A., Hughes, T. J., and Landis, C. M., 2012. "A phase-field description of dynamic brittle fracture". *Computer Methods in Applied Mechanics and Engineering,* **217**, pp. 77–95.

[159] Borden, M. J., Hughes, T. J., Landis, C. M., and Verhoosel, C. V., 2014. "A higher-order phase-field model for brittle fracture: Formulation and analysis within the isogeometric analysis framework". *Computer Methods in Applied Mechanics and Engineering,* **273**, pp. 100–118.

[160] Mesgarnejad, A., Bourdin, B., and Khonsari, M., 2015. "Validation simulations for the variational approach to fracture". *Computer Methods in Applied Mechanics and Engineering,* **290**, pp. 420–437.

[161] Borden, M. J., Hughes, T. J., Landis, C. M., Anvari, A., and Lee, I. J., 2016. "A phase-field formulation for fracture in ductile materials: Finite deformation balance law derivation, plastic degradation, and stress triaxiality effects". *Computer Methods in Applied Mechanics and Engineering,* **312**, pp. 130–166.

[162] Liu, G., Li, Q., Msekh, M. A., and Zuo, Z., 2016. "Abaqus implementation of monolithic and staggered schemes for quasi-static and dynamic fracture phase-field model". *Computational Materials Science,* **121**, pp. 35–47.

[163] Gültekin, O., Dal, H., and Holzapfel, G. A., 2016. "A phase-field approach to model fracture of arterial walls: theory and finite element analysis". *Computer methods in applied mechanics and engineering,* **312**, pp. 542–566.

[164] Pham, K., and Ravi-Chandar, K., 2017. "The formation and growth of echelon cracks in brittle materials". *International Journal of Fracture,* **206**(2), pp. 229–244.

[165] Miehe, C., and Schänzel, L.-M., 2014. "Phase field modeling of fracture in rubbery polymers. part i: Finite elasticity coupled with brittle failure". *Journal of the Mechanics and Physics of Solids,* **65**, pp. 93–113.

[166] Hesch, C., and Weinberg, K., 2014. "Thermodynamically consistent algorithms for a finite-deformation phase-field approach to fracture". *International Journal for Numerical Methods in Engineering,* **99**(12), pp. 906–924.

[167] Raina, A., and Miehe, C., 2016. "A phase-field model for fracture in biological tissues". *Biomechanics and modeling in mechanobiology,* **15**(3), pp. 479–496.

[168] Ambati, M., and De Lorenzis, L., 2016. "Phase-field modeling of brittle and ductile fracture in shells with isogeometric nurbs-based solid-shell elements". *Computer Methods in Applied Mechanics and Engineering,* **312**, pp. 351–373.

[169] Hesch, C., Gil, A., Ortigosa, R., Dittmann, M., Bilgen, C., Betsch, P., Franke, M., Janz, A., and Weinberg, K., 2017. "A framework for polyconvex large strain phase-field methods to fracture". *Computer Methods in Applied Mechanics and Engineering,* **317**, pp. 649–683.

[170] Lee, S., Yoon, H. C., and Muddamallappa, M. S., 2020. Nonlinear strain-limiting elasticity for fracture propagation with phase-field approach.

[171] Bourdin, B., Larsen, C. J., and Richardson, C. L., 2011. "A time-discrete model for dynamic fracture based on crack regularization". *International journal of fracture,* **168**(2), pp. 133–143.

[172] Schlüter, A., Willenbücher, A., Kuhn, C., and Müller, R., 2014. "Phase field approximation of dynamic brittle fracture". *Computational Mechanics,* **54**(5), pp. 1141–1161.

[173] Li, T., Marigo, J.-J., Guilbaud, D., and Potapov, S., 2016. "Gradient damage modeling of brittle fracture in an explicit dynamics context". *International Journal for Numerical Methods in Engineering,* **108**(11), pp. 1381–1405.

[174] Roubicek, T., 2019. Models of dynamic damage and phase-field fracture, and their various time discretisations.

[175] Geelen, R. J., Liu, Y., Hu, T., Tupek, M. R., and Dolbow, J. E., 2019. "A phase-field formulation for dynamic cohesive fracture". *Computer Methods in Applied Mechanics and Engineering,* **348**, May, p. 680–711.

[176] Verhoosel, C. V., and de Borst, R., 2013. "A phase-field model for cohesive fracture". *International Journal for numerical methods in Engineering,* **96**(1), pp. 43–62.

[177] May, S., Vignollet, J., and De Borst, R., 2015. "A numerical assessment of phase-field models for brittle and cohesive fracture: γ-convergence and stress oscillations". *European Journal of Mechanics-A/Solids,* **52**, pp. 72–84.

[178] Nguyen, T. T., Yvonnet, J., Zhu, Q.-Z., Bornert, M., and Chateau, C., 2016. "A phase-field method for computational modeling of interfacial damage interacting with crack propagation in realistic microstructures obtained by microtomography". *Computer Methods in Applied Mechanics and Engineering,* **312**, pp. 567–595.

[179] Vignollet, J., May, S., De Borst, R., and Verhoosel, C. V., 2014. "Phase-field models for brittle and cohesive fracture". *Meccanica,* **49**(11), pp. 2587–2601.

[180] Duda, F. P., Ciarbonetti, A., Sánchez, P. J., and Huespe, A. E., 2015. "A phase-field/gradient damage model for brittle fracture in elastic–plastic solids". *International Journal of Plasticity,* **65**, pp. 269–296.

[181] Alessi, R., Marigo, J.-J., and Vidoli, S., 2015. "Gradient damage models coupled with plasticity: variational formulation and main properties". *Mechanics of Materials,* **80**, pp. 351–367.

[182] Ambati, M., Kruse, R., and De Lorenzis, L., 2016. "A phase-field model for ductile fracture at finite strains and its experimental verification". *Computational Mechanics,* **57**(1), pp. 149–167.

[183] Ambati, M., Gerasimov, T., and De Lorenzis, L., 2015. "Phase-field modeling of ductile fracture". *Computational Mechanics,* **55**(5), pp. 1017–1040.

[184] Kuhn, C., Noll, T., and Müller, R., 2016. "On phase field modeling of ductile fracture". *GAMM-Mitteilungen,* **39**(1), pp. 35–54.

[185] Bleyer, J., and Alessi, R., 2018. "Phase-field modeling of anisotropic brittle fracture including several damage mechanisms". *Computer Methods in Applied Mechanics and Engineering,* **336**, pp. 213–236.

[186] Hakim, V., and Karma, A., 2005. "Crack path prediction in anisotropic brittle materials". *Physical review letters,* **95**(23), p. 235501.

[187] Clayton, J. D., and Knap, J., 2014. "A geometrically nonlinear phase field theory of brittle fracture". *International Journal of Fracture,* **189**(2), pp. 139–148.

[188] Li, B., Peco, C., Millán, D., Arias, I., and Arroyo, M., 2015. "Phase-field modeling and simulation of fracture in brittle materials with strongly anisotropic surface energy". *International Journal for Numerical Methods in Engineering,* **102**(3-4), pp. 711–727.

[189] Nguyen, T. T., Réthoré, J., and Baietto, M.-C., 2017. "Phase field modelling of anisotropic crack propagation". *European Journal of Mechanics-A/Solids,* **65**, pp. 279–288.

[190] Teichtmeister, S., Kienle, D., Aldakheel, F., and Keip, M.-A., 2017. "Phase field modeling of fracture in anisotropic brittle solids". *International Journal of Non-Linear Mechanics,* **97**, pp. 1–21.

[191] Mesgarnejad, A., Bourdin, B., and Khonsari, M., 2013. "A variational approach to the fracture of brittle thin films subject to out-of-plane loading". *Journal of the Mechanics and Physics of Solids,* **61**(11), pp. 2360–2379.

[192] Baldelli, A. L., Babadjian, J.-F., Bourdin, B., Henao, D., and Maurini, C., 2014. "A variational model for fracture and debonding of thin films under in-plane loadings". *Journal of the Mechanics and Physics of Solids,* **70**, pp. 320–348.

[193] Hansen-Dörr, A. C., de Borst, R., Hennig, P., and Kästner, M., 2019. "Phase-field modelling of interface failure in brittle materials". *Computer Methods in Applied Mechanics and Engineering,* **346**, pp. 25–42.

[194] Patil, R., Mishra, B., Singh, I., and Bui, T., 2018. "A new multiscale phase field method to simulate failure in composites". *Advances in Engineering Software,* **126**, pp. 9–33.

[195] Quintanas-Corominas, A., Reinoso, J., Casoni, E., Turon, A., and Mayugo, J., 2019. "A phase field approach to simulate intralaminar and translaminar fracture in long fiber composite materials". *Composite Structures,* **220**, pp. 899–911.

[196] Song, L., Meng, S., Xu, C., Fang, G., and Yang, Q., 2019. "Finite element-based phase-field simulation of interfacial damage in unidirectional composite under transverse tension". *Modelling and Simulation in Materials Science and Engineering,* **27**(5), p. 055011.

[197] Spatschek, R., Pilipenko, D., Müller-Gugenberger, C., and Brener, E. A., 2006. "Phase field modeling of fracture and composite materials". *Phys Rev Lett,* **96**, p. 015502.

[198] Denli, F. A., Gültekin, O., Holzapfel, G. A., and Dal, H., 2020. "A phase-field model for fracture of unidirectional fiber-reinforced polymer matrix composites". *Computational Mechanics*, pp. 1–18.

[199] Amor, H., Marigo, J.-J., and Maurini, C., 2009. "Regularized formulation of the variational brittle fracture with unilateral contact: Numerical experiments". *Journal of the Mechanics and Physics of Solids,* **57**(8), pp. 1209–1229.

[200] Zhang, X., Sloan, S. W., Vignes, C., and Sheng, D., 2017. "A modification of the phase-field model for mixed mode crack propagation in rock-like materials". *Computer Methods in Applied Mechanics and Engineering,* **322**, pp. 123–136.

[201] Strobl, M., and Seelig, T., 2015. "A novel treatment of crack boundary conditions in phase field models of fracture". *Pamm,* **15**(1), pp. 155–156.

[202] Steinke, C., and Kaliske, M., 2019. "A phase-field crack model based on directional stress decomposition". *Computational Mechanics,* **63**(5), pp. 1019–1046.

[203] Bryant, E. C., and Sun, W., 2018. "A mixed-mode phase field fracture model in anisotropic rocks with consistent kinematics". *Computer Methods in Applied Mechanics and Engineering,* **342**, pp. 561–584.

[204] Freddi, F., and Royer-Carfagni, G., 2010. "Regularized variational theories of fracture: a unified approach". *Journal of the Mechanics and Physics of Solids,* **58**(8), pp. 1154–1174.

[205] Bilgen, C., Homberger, S., and Weinberg, K., 2019. "Phase-field fracture simulations of the brazilian splitting test". *International Journal of Fracture,* **220**, pp. 85–98.

[206] Fan, M., Jin, Y., and Wick, T., 2019. A phase-field model for mixed-mode fracture. Hannover : Institutionelles Repositorium der Leibniz Universität Hannover, 2019, 40 S. DOI: https://doi.org/10.15488/5369.

[207] Bleyer, J., Roux-Langlois, C., and Molinari, J.-F., 2017. "Dynamic crack propagation with a variational phase-field model: limiting speed, crack branching and velocity-toughening mechanisms". *International Journal of Fracture,* **204**(1), pp. 79–100.

[208] Mang, K., Wick, T., and Wollner, W., 2020. "A phase-field model for fractures in nearly incom-

pressible solids". *Computational Mechanics,* **65**, pp. 61–78.

[209] Basava, S., Mang, K., Walloth, M., Wick, T., and Wollner, W., 2020. Adaptive and pressure-robust discretization of incompressible pressure-driven phase-field fracture. submitted, SPP 1748 final report.

[210] Ulmer, H., Hofacker, M., and Miehe, C., 2012. "Phase field modeling of fracture in plates and shells". *PAMM,* **12**(1), pp. 171–172.

[211] Amiri, F., Millán, D., Shen, Y., Rabczuk, T., and Arroyo, M., 2014. "Phase-field modeling of fracture in linear thin shells". *Theoretical and Applied Fracture Mechanics,* **69**, pp. 102–109.

[212] Areias, P., Rabczuk, T., and Msekh, M., 2016. "Phase-field analysis of finite-strain plates and shells including element subdivision". *Computer Methods in Applied Mechanics and Engineering,* **312**, pp. 322–350.

[213] Reinoso, J., Paggi, M., and Linder, C., 2017. "Phase field modeling of brittle fracture for enhanced assumed strain shells at large deformations: formulation and finite element implementation". *Computational Mechanics,* **59**(6), pp. 981–1001.

[214] Kuhn, C., and Müller, R., 2009. "Phase field simulation of thermomechanical fracture". In PAMM: Proceedings in Applied Mathematics and Mechanics, Vol. 9, Wiley Online Library, pp. 191–192.

[215] Kuhn, C., and Müller, R., 2010. "A continuum phase field model for fracture". *Engineering Fracture Mechanics,* **77**(18), pp. 3625–3634.

[216] Miehe, C., Hofacker, M., and Welschinger, F., 2010. "A phase field model for rate-independent crack propagation: Robust algorithmic implementation based on operator splits". *Computer Methods in Applied Mechanics and Engineering,* **199**(45-48), pp. 2765–2778.

[217] Wheeler, M., Wick, T., and Wollner, W., 2014. "An augmented-Lagangrian method for the phase-field approach for pressurized fractures". *Comp. Meth. Appl. Mech. Engrg.,* **271**, pp. 69–85.

[218] Heister, T., Wheeler, M. F., and Wick, T., 2015. "A primal-dual active set method and predictor-corrector mesh adaptivity for computing fracture propagation using a phase-field approach". *Computer Methods in Applied Mechanics and Engineering,* **290**, pp. 466–495.

[219] Wambacq, J., Ulloa, J., Lombaert, G., and François, S., 2020. Interior-point methods for the phase-field approach to brittle and ductile fracture.

[220] Gerasimov, T., and Lorenzis, L. D., 2019. "On penalization in variational phase-field models of brittle fracture". *Computer Methods in Applied Mechanics and Engineering,* **354**, pp. 990 – 1026.

[221] Burke, S., Ortner, C., and Süli, E., 2010. "An adaptive finite element approximation of a variational model of brittle fracture". *SIAM J. Numer. Anal.,* **48**(3), pp. 980–1012.

[222] Bourdin, B., 2007. "Numerical implementation of a variational formulation of quasi-static brittle fracture". *Interfaces Free Bound.,* **9**(3), 08, pp. 411–430.

[223] Farrell, P., and Maurini, C., 2017. "Linear and nonlinear solvers for variational phase-field models of brittle fracture". *International Journal for Numerical Methods in Engineering,* **109**(5), pp. 648–667.

[224] Wu, J.-Y., 2018. "A geometrically regularized gradient-damage model with energetic equivalence". *Computer Methods in Applied Mechanics and Engineering,* **328**, pp. 612–637.

[225] Wu, J.-Y., 2018. "Robust numerical implementation of non-standard phase-field damage models for failure in solids". *Computer Methods in Applied Mechanics and Engineering,* **340**, pp. 767–797.

[226] Brun, M. K., Wick, T., Berre, I., Nordbotten, J. M., and Radu, F. A., 2020. "An iterative staggered scheme for phase field brittle fracture propagation with stabilizing parameters". *Computer Methods in Applied Mechanics and Engineering,* **361**, p. 112752.

[227] Storvik, E., Both, J. W., Sargado, J. M., Nordbotten, J. M., and Radu, F. A., 2020. An accelerated staggered scheme for phase-field modeling of brittle fracture.

[228] Jammoul, M., Wheeler, M. F., and Wick, T., 2020. "A phase-field multirate scheme with stabilized iterative coupling for pressure driven fracture propagation in porous media". *Computers & Mathematics with Applications*.

[229] Engwer, C., Pop, I. S., and Wick, T., 2019. Dynamic and weighted stabilizations of the l-scheme applied to a phase-field model for fracture propagation.

[230] Gerasimov, T., and De Lorenzis, L., 2016. "A line search assisted monolithic approach for phase-field computing of brittle fracture". *Computer Methods in Applied Mechanics and Engineering,* **312**, pp. 276–303.

[231] Wick, T., 2017. "Modified Newton methods for solving fully monolithic phase-field quasi-static brittle fracture propagation". *Computer Methods in Applied Mechanics and Engineering,* **325**, pp. 577 – 611.

[232] Wick, T., 2017. "An error-oriented Newton/inexact augmented Lagrangian approach for fully monolithic phase-field fracture propagation". *SIAM Journal on Scientific Computing,* **39**(4), pp. B589–B617.

[233] Jodlbauer, D., Langer, U., and Wick, T., 2020. "Matrix-free multigrid solvers for phase-field fracture problems". *Computer Methods in Applied Mechanics and Engineering,* **372**, p. 113431.

[234] Kopanicakova, A., and Krause, R., 2020. "A recursive multilevel trust region method with application to fully monolithic phase-field models of brittle fracture". *Computer Methods in Applied Mechanics and Engineering,* **360**, p. 112720.

[235] May, S., Vignollet, J., and de Borst, R., 2016. "A new arc-length control method based on the rates of the internal and the dissipated energy". *Engineering Computations,* **33**(1), pp. 100–115.

[236] Singh, N., Verhoosel, C., De Borst, R., and Van Brummelen, E., 2016. "A fracture-controlled path-following technique for phase-field modeling of brittle fracture". *Finite Elements in Analysis and Design,* **113**, pp. 14–29.

[237] Heister, T., and Wick, T., 2018. "Parallel solution, adaptivity, computational convergence, and open-source code of 2d and 3d pressurized phase-field fracture problems". *PAMM,* **18**(1), p. e201800353.

[238] Jodlbauer, D., Langer, U., and Wick, T., 2020. "Parallel matrix-free higher-order finite element solvers for phase-field fracture problems". *Mathematical and Computational Applications,* **25**(3), p. 40.

[239] Nguyen, T. T., Yvonnet, J., Zhu, Q.-Z., Bornert, M., and Chateau, C., 2015. "A phase field method to simulate crack nucleation and propagation in strongly heterogeneous materials from direct imaging of their microstructure". *Engineering Fracture Mechanics,* **139**, pp. 18–39.

[240] Noii, N., Aldakheel, F., Wick, T., and Wriggers, P., 2020. "An adaptive global-local approach for phase-field modeling of anisotropic brittle fracture". *Computer Methods in Applied Mechanics and Engineering,* **361**, p. 112744.

[241] Zavattieri, P. D., 2006. "Modeling of crack propagation in thin-walled structures using a cohesive model for shell elements". *Journal of applied mechanics,* **73**(6), pp. 948–958.

[242] Kuhn, C., Schlüter, A., and Müller, R., 2015. "On degradation functions in phase field fracture models". *Computational Materials Science,* **108**, pp. 374–384.

[243] Steinke, C., Özenç, K., Chinaryan, G., and Kaliske, M., 2016. "A comparative study of the r-adaptive material force approach and the phase-field method in dynamic fracture". *International Journal of Fracture,* **201**(1), pp. 97–118.

[244] Msekh, M. A., Sargado, J. M., Jamshidian, M., Areias, P. M., and Rabczuk, T., 2015. "Abaqus implementation of phase-field model for brittle fracture". *Computational Materials Science,* **96**, pp. 472–484.

[245] Molnár, G., and Gravouil, A., 2017. "2d and 3d abaqus implementation of a robust staggered phase-field solution for modeling brittle fracture". *Finite Elements in Analysis and Design,* **130**, pp. 27–38.

[246] Pillai, U., Heider, Y., and Markert, B., 2018. "A diffusive dynamic brittle fracture model for heterogeneous solids and porous materials with implementation using a user-element subroutine". *Computational Materials Science,* **153**, pp. 36–47.

[247] Bhowmick, S., and Liu, G. R., 2018. "A phase-field modeling for brittle fracture and crack propagation based on the cell-based smoothed finite element method". *Engineering Fracture Mechanics,* **204**, pp. 369–387.

[248] Jeong, H., Signetti, S., Han, T.-S., and Ryu, S., 2018. "Phase field modeling of crack propagation under combined shear and tensile loading with hybrid formulation". *Computational Materials Science,* **155**, pp. 483–492.

[249] van Zwieten, G., van Zwieten, J., Verhoosel, C., Fonn, E., van Opstal, T., and Hoitinga, W., 2019. Nutils, June.

[250] Chakraborty, P., Sabharwall, P., and Carroll, M. C., 2016. "A phase-field approach to model multi-axial and microstructure dependent fracture in nuclear grade graphite". *Journal of Nuclear Materials,* **475**, pp. 200–208.

[251] Gaston, D., Newman, C., Hansen, G., and Lebrun-Grandie, D., 2009. "Moose: A parallel computational framework for coupled systems of nonlinear equations". *Nuclear Engineering and Design,* **239**(10), pp. 1768–1778.

[252] Heister, T., and Wick, T., 2020. "pfm-cracks: A parallel-adaptive framework for phase-field fracture propagation". *Software Impacts,* **6**, p. 100045.

[253] Klinsmann, M., Rosato, D., Kamlah, M., and McMeeking, R. M., 2015. "An assessment of the phase field formulation for crack growth". *Computer Methods in Applied Mechanics and Engineering,* **294**, pp. 313–330.

[254] Alnæs, M., Blechta, J., Hake, J., Johansson, A., Kehlet, B., Logg, A., Richardson, C., Ring, J., Rognes, M. E., and Wells, G. N., 2015. "The fenics project version 1.5". *Archive of Numerical Software,* **3**(100).

[255] Ziaei-Rad, V., and Shen, Y., 2016. "Massive parallelization of the phase field formulation for crack propagation with time adaptivity". *Computer Methods in Applied Mechanics and Engineering,* **312**, pp. 224–253.

[256] Bourdin, B., 2019. bourdin/mef90 0.1.0, June.

[257] Burke, S., Ortner, C., and Süli, E., 2013. "An adaptive finite element approximation of a generalized Ambrosio-Tortorelli functional". *M3AS,* **23**(9), pp. 1663–1697.

[258] Mang, K., Walloth, M., Wick, T., and Wollner, W., 2020. "Mesh adaptivity for quasi-static phase-field fractures based on a residual-type a posteriori error estimator". *GAMM-Mitteilungen,* **43**(1), p. e202000003.

[259] Wick, T., 2016. "Goal functional evaluations for phase-field fracture using pu-based dwr mesh adaptivity". *Computational Mechanics,* **57**(6), pp. 1017–1035.

[260] Artina, M., Fornasier, M., Micheletti, S., and Perotto, S., 2015. "Anisotropic mesh adaptation for crack detection in brittle materials". *SIAM Journal on Scientific Computing,* **37**(4), pp. B633–B659.

[261] Borden, M. J., Verhoosel, C. V., Scott, M. A., Hughes, T. J. R., and Landis, C. M., 2012. "A phase-field description of dynamic brittle fracture". *Comput. Meth. Appl. Mech. Engrg.,* **217**, pp. 77–95.

[262] Andersson, J., and Mikayelyan, H., 2012. "The asymptotics of the curvature of the free discontinuity set near the cracktip for the minimizers of the mumford-shah functional in the plain". *arXiv preprint arXiv:1204.5328*.

[263] Bonnet, A., and David, G., 2001. *Cracktip is a global Mumford-Shah minimizer*. Société mathématique de France.

[264] Bellettini, G., and Coscia, A., 1994. "Discrete approximation of a free discontinuity problem". *Numerical Functional Analysis and Optimization,* **15**(3-4), pp. 201–224.

[265] Schröder, J., Wick, T., Reese, S., Wriggers, P., Müller, R., Kollmannsberger, S., Kästner, M., Schwarz, A., Igelbüscher, M., Viebahn, N., Bayat, H. R., Wulfinghoff, S., Mang, K., Rank, E., Bog, T., d'Angella, D., Elhaddad, M., Hennig, P., Düster, A., Garhuom, W., Hubrich, S., Walloth, M., Wollner, W., Kuhn, C., and Heister, T., 2020. "A selection of benchmark problems in solid mechanics and applied mathematics". *Arch Computat Methods Eng*.

[266] Negri, M., 1999. "The anisotropy introduced by the mesh in the finite element approximation of the mumford-shah functional". *Numerical Functional Analysis and Optimization,* **20**(9-10), pp. 957–982.

[267] Linse, T., Hennig, P., Kästner, M., and de Borst, R., 2017. "A convergence study of phase-field models for brittle fracture". *Engineering Fracture Mechanics,* **184**, pp. 307–318.

[268] Badnava, H., Msekh, M. A., Etemadi, E., and Rabczuk, T., 2018. "An h-adaptive thermo-mechanical phase field model for fracture". *Finite Elements in Analysis and Design,* **138**, pp. 31 – 47.

[269] Patil, R., Mishra, B., and Singh, I., 2018. "An adaptive multiscale phase field method for brittle fracture". *Computer Methods in Applied Mechanics and Engineering,* **329**, pp. 254 – 288.

[270] Wick, T., 2017. "Coupling fluid-structure interaction with phase-field fracture: algorithmic details". In *Fluid-Structure Interaction: Modeling, Adaptive Discretization and Solvers*, S. Frei, B. Holm, T. Richter, T. Wick, and H. Yang, eds., Radon Series on Computational and Applied Mathematics. Walter de Gruyter, Berlin.

[271] Gerasimov, T., Noii, N., Allix, O., and De Lorenzis, L., 2018. "A non-intrusive global/local approach applied to phase-field modeling of brittle fracture". *Advanced Modeling and Simulation in Engineering Sciences,* **5**(1), May, p. 14.

[272] Aldakheel, F., Noii, N., Wick, T., and Wriggers, P., 2020, accepted for publication in Computers and Mathematics with Applications (CAMWA). A global-local approach for hydraulic phase-field fracture in poroelastic media.

[273] Aldakheel, F., Noii, N., Wick, T., Allix, O., and Wriggers, P., 2021. Multilevel global-local techniques for adaptive ductile phase-field fracture.

[274] Gräser, C., Kienle, D., and Sander, O., 2021. Truncated nonsmooth newton multigrid for phase-field brittle-fracture problems.

[275] Zhang, X., Vignes, C., Sloan, S. W., and Sheng, D., 2017. "Numerical evaluation of the phase-field model for brittle fracture with emphasis on the length scale". *Computational Mechanics,* **59**(5), pp. 737–752.

[276] Zhuang, X., Zhou, S., Sheng, M., and Li, G., 2020. "On the hydraulic fracturing in naturally-layered porous media using the phase field method". *Engineering Geology,* **266**, p. 105306.

[277] Noll, T., Kuhn, C., Olesch, D., and Müller, R., 2019. "3d phase field simulations of ductile fracture". *GAMM-Mitteilungen*, p. e202000008.

[278] Chukwudozie, C., Bourdin, B., and Yoshioka, K., 2019. "A variational phase-field model for hydraulic fracturing in porous media". *Computer Methods in Applied Mechanics and Engineering,* **347**, pp. 957–982.

[279] Haslach Jr, H. W., 2011. *Maximum dissipation non-equilibrium thermodynamics and its geometric structure*. Springer Science & Business Media.

[280] Ulmer, H., Hofacker, M., and Miehe, C., 2013. "Phase field modeling of brittle and ductile fracture". *PAMM,* **13**(1), pp. 533–536.

[281] Mauthe, S., and Miehe, C., 2015. "Phase-field modeling of hydraulic fracture". *PAMM,* **15**(1), pp. 141–142.

[282] Miehe, C., Teichtmeister, S., and Aldakheel, F., 2016. "Phase-field modelling of ductile fracture: a variational gradient-extended plasticity-damage theory and its micromorphic regularization". *Philosophical Transactions of the Royal Society A: Mathematical, Physical and Engineering Sciences,* **374**(2066), p. 20150170.

[283] Roy, P., Pathrikar, A., Deepu, S., and Roy, D., 2017. "Peridynamics damage model through phase field theory". *International Journal of Mechanical Sciences,* **128**, pp. 181–193.

[284] Farrahi, G. H., Javanbakht, M., and Jafarzadeh, H., 2018. "On the phase field modeling of crack growth and analytical treatment on the parameters". *Continuum Mechanics and Thermodynamics*, pp. 1–18.

[285] Alessi, R., Marigo, J.-J., Maurini, C., and Vidoli, S., 2018. "Coupling damage and plasticity for a phase-field regularisation of brittle, cohesive and ductile fracture: one-dimensional examples". *International Journal of Mechanical Sciences,* **149**, pp. 559–576.

[286] Devore, J. L., 2011. *Probability and Statistics for Engineering and the Sciences*. Cengage learning.

[287] Virtanen, P., Gommers, R., Oliphant, T. E., Haberland, M., Reddy, T., Cournapeau, D., Burovski, E., Peterson, P., Weckesser, W., Bright, J., van der Walt, S. J., Brett, M., Wilson, J., Jarrod Millman, K., Mayorov, N., Nelson, A. R. J., Jones, E., Kern, R., Larson, E., Carey, C., Polat, İ., Feng, Y., Moore, E. W., Vand erPlas, J., Laxalde, D., Perktold, J., Cimrman, R., Henriksen, I., Quintero, E. A., Harris, C. R., Archibald, A. M., Ribeiro, A. H., Pedregosa, F., van Mulbregt, P., and Contributors, S. . ., 2020. "Scipy 1.0: Fundamental algorithms for scientific computing in python". *Nature Methods*.

[288] Boyce, B. L., Kramer, S. L., Fang, H. E., Cordova, T. E., Neilsen, M. K., Dion, K., Kaczmarowski, A. K., Karasz, E., Xue, L., Gross, A. J., et al., 2014. "The sandia fracture challenge: blind round robin predictions of ductile tearing". *International Journal of Fracture,* **186**(1-2), pp. 5–68.

[289] Behzadinasab, M., and Foster, J. T. "Revisiting the third sandia fracture challenge: a bondassociated, semi-lagrangian peridynamic approach to modeling large deformation and ductile fracture". *International Journal of Fracture*.

[290] Dittmann, M., Aldakheel, F., Schulte, J., Wriggers, P., and Hesch, C., 2018. "Variational phase-field formulation of non-linear ductile fracture". *Computer Methods in Applied Mechanics and Engineering,* **342**, pp. 71–94.

[291] Kramer, S. L., Jones, A., Mostafa, A., Ravaji, B., Tancogne-Dejean, T., Roth, C. C., Bandpay, M. G., Pack, K., Foster, J. T., Behzadinasab, M., et al., 2019. "The third sandia fracture challenge: predictions of ductile fracture in additively manufactured metal". *International Journal of Fracture,* **218**(1-2), pp. 5–61.

[292] Hocine, N. A., Abdelaziz, M. N., and Mesmacque, G., 1998. "Experimental and numerical investigation on single specimen methods of determination of j in rubber materials". *International Journal of Fracture,* **94**(4), pp. 321–338.

[293] Talamini, B., Mao, Y., and Anand, L., 2018. "Progressive damage and rupture in polymers". *Journal of the Mechanics and Physics of Solids,* **111**, pp. 434–457.

[294] Behera, D., Roy, P., and Madenci, E., 2020. "Peridynamic correspondence model for finite elastic deformation and rupture in neo-hookean materials". *International Journal of Non-Linear Mechanics,* **126**, p. 103564.

[295] Sundaram, B. M., and Tippur, H. V., 2018. "Dynamic fracture of soda-lime glass: A full-field optical investigation of crack initiation, propagation and branching". *Journal of the Mechanics and Physics of Solids,* **120**, pp. 132–153.

[296] Mehrmashhadi, J., Bahadori, M., and Bobaru, F., 2020. "On validating peridynamic models and a phase-field model for dynamic brittle fracture in glass". *Engineering Fracture Mechanics*, p. 107355.

[297] Ren, B., and Wu, C., 2018. "A peridynamic model for damage prediction fiber-reinforced composite laminate". In 15th International LS-DYNA User Conference, p. 10.

[298] Dayal, K., and Bhattacharya, K., 2006. "Kinetics of phase transformations in the peridynamic formulation of continuum mechanics". *Journal of the Mechanics and Physics of Solids,* **54**(9), pp. 1811–1842.

[299] Huang, D., Lu, G., and Qiao, P., 2015. "An improved peridynamic approach for quasi-static elastic deformation and brittle fracture analysis". *International Journal of Mechanical Sciences,* **94**, pp. 111–122.

[300] Mikata, Y., 2012. "Analytical solutions of peristatic and peridynamic problems for a 1d infinite rod". *International Journal of Solids and Structures,* **49**(21), pp. 2887–2897.

[301] Zaccariotto, M., Luongo, F., Galvanetto, U., et al., 2015. "Examples of applications of the peridynamic theory to the solution of static equilibrium problems". *The Aeronautical Journal,* **119**(1216), pp. 677–700.

[302] Buryachenko, V. A., Wanji, C., and Shengqi, Y., 2015. "Effective thermoelastic properties of heterogeneous thermoperistatic bar of random structure". *International Journal for Multiscale Computational Engineering,* **13**(1).

[303] Hofacker, M., and Miehe, C., 2013. "A phase field model of dynamic fracture: Robust field updates for the analysis of complex crack patterns". *International Journal for Numerical Methods in Engineering,* **93**(3), pp. 276–301.

[304] Noll, T., Kuhn, C., and Müller, R., 2017. "A monolithic solution scheme for a phase field model of ductile fracture". *PAMM,* **17**(1), pp. 75–78.

[305] Tanné, E., Li, T., Bourdin, B., Marigo, J.-J., and Maurini, C., 2018. "Crack nucleation in variational phase-field models of brittle fracture". *Journal of the Mechanics and Physics of Solids,* **110**, pp. 80–99.

[306] Sneddon, I. N., and Lowengrub, M., 1969. *Crack problems in the classical theory of elasticity*. SIAM series in Applied Mathematics. John Wiley and Sons, Philadelphia.

[307] Goswami, S., Anitescu, C., Chakraborty, S., and Rabczuk, T., 2020. "Transfer learning enhanced physics informed neural network for phase-field modeling of fracture". *Theoretical and Applied Fracture Mechanics,* **106**, p. 102447.

[308] Nguyen, C. T., Oterkus, S., and Oterkus, E., 2021. "A physics-guided machine learning model for two-dimensional structures based on ordinary state-based peridynamics". *Theoretical and Applied Fracture Mechanics,* **112**, p. 102872.

[309] Stochino, F., Qinami, A., and Kaliske, M., 2017. "Eigenerosion for static and dynamic brittle fracture". *Engineering Fracture Mechanics,* **182**, pp. 537–551.

[310] Pandolfi, A., and Ortiz, M., 2012. "An eigenerosion approach to brittle fracture". *International Journal for Numerical Methods in Engineering,* **92**(8), pp. 694–714.

[311] Pandolfi, A., Li, B., and Ortiz, M., 2013. "Modeling fracture by material-point erosion". *International Journal of fracture,* **184**(1-2), pp. 3–16.

[312] Wang, K., and Sun, W., 2017. "A unified variational eigen-erosion framework for interacting brittle fractures and compaction bands in fluid-infiltrating porous media". *Computer Methods in Applied Mechanics and Engineering,* **318**, pp. 1–32.

[313] Bobaru, F., and Duangpanya, M., 2010. "The peridynamic formulation for transient heat conduction". *International Journal of Heat and Mass Transfer,* **53**(19-20), pp. 4047–4059.

[314] Oterkus, S., Madenci, E., and Agwai, A., 2014. "Peridynamic thermal diffusion". *Journal of Computational Physics,* **265**, pp. 71–96.

[315] Oterkus, S., Madenci, E., and Agwai, A., 2014. "Fully coupled peridynamic thermomechanics". *Journal of the Mechanics and Physics of Solids,* **64**, pp. 1–23.

[316] Chen, Z., and Bobaru, F., 2015. "Selecting the kernel in a peridynamic formulation: a study for transient heat diffusion". *Computer Physics Communications,* **197**, pp. 51–60.

[317] Liao, Y., Liu, L., Liu, Q., Lai, X., Assefa, M., and Liu, J., 2017. "Peridynamic simulation of transient heat conduction problems in functionally gradient materials with cracks". *Journal of Thermal Stresses,* **40**(12), pp. 1484–1501.

[318] Diyaroglu, C., Oterkus, S., Oterkus, E., Madenci, E., Han, S., and Hwang, Y., 2017. "Peridynamic wetness approach for moisture concentration analysis in electronic packages". *Microelectronics Reliability,* **70**, pp. 103–111.

[319] Tao, Y., Tian, X., and Du, Q., 2017. "Nonlocal diffusion and peridynamic models with neumann type constraints and their numerical approximations". *Applied Mathematics and Computation,* **305**, pp. 282–298.

[320] Gu, X., Zhang, Q., and Madenci, E., 2019. "Refined bond-based peridynamics for thermal diffusion". *Engineering Computations*.

[321] Hattori, G., Trevelyan, J., Augarde, C. E., Coombs, W. M., and Aplin, A. C., 2017. "Numerical simulation of fracking in shale rocks: current state and future approaches". *Archives of Computational Methods in Engineering,* **24**(2), pp. 281–317.

[322] Ouchi, H., Katiyar, A., York, J., Foster, J. T., and Sharma, M. M., 2015. "A fully coupled porous flow and geomechanics model for fluid driven cracks: a peridynamics approach". *Computational Mechanics,* **55**(3), pp. 561–576.

[323] Wang, Y., Zhou, X., and Xu, X., 2016. "Numerical simulation of propagation and coalescence of flaws in rock materials under compressive loads using the extended non-ordinary state-based peridynamics". *Engineering Fracture Mechanics,* **163**, pp. 248–273.

[324] Zhou, X., and Shou, Y., 2016. "Numerical simulation of failure of rock-like material subjected to compressive loads using improved peridynamic method". *International Journal of Geomechanics,* **17**(3), p. 04016086.

[325] Zhou, X.-P., Gu, X.-B., and Wang, Y.-T., 2015. "Numerical simulations of propagation, bifurcation and coalescence of cracks in rocks". *international journal of Rock Mechanics and Mining Sciences,* **80**, pp. 241–254.

[326] Ren, B., Fan, H., Bergel, G. L., Regueiro, R. A., Lai, X., and Li, S., 2015. "A peridynamics–sph coupling approach to simulate soil fragmentation induced by shock waves". *Computational Mechanics,* **55**(2), pp. 287–302.

[327] Fan, H., and Li, S., 2017. "A peridynamics-sph modeling and simulation of blast fragmentation of soil under buried explosive loads". *Computer methods in applied mechanics and engineering,* **318**, pp. 349–381.

[328] Nadimi, S., Miscovic, I., and McLennan, J., 2016. "A 3d peridynamic simulation of hydraulic fracture

process in a heterogeneous medium". *Journal of Petroleum Science and Engineering,* **145**, pp. 444–452.

[329] Wu, F., Li, S., Duan, Q., and Li, X., 2016. "Application of the method of peridynamics to the simulation of hydraulic fracturing process". In International Conference on Discrete Element Methods, Springer, pp. 561–569.

[330] Panchadhara, R., Gordon, P. A., and Parks, M. L., 2017. "Modeling propellant-based stimulation of a borehole with peridynamics". *International Journal of Rock Mechanics and Mining Sciences,* **93**, pp. 330–343.

[331] Lai, X., Ren, B., Fan, H., Li, S., Wu, C., Regueiro, R. A., and Liu, L., 2015. "Peridynamics simulations of geomaterial fragmentation by impulse loads". *International Journal for Numerical and Analytical Methods in Geomechanics,* **39**(12), pp. 1304–1330.

[332] Yan, F., Feng, X.-T., Pan, P.-Z., and Li, S.-J., 2014. "A continuous-discontinuous cellular automaton method for cracks growth and coalescence in brittle material". *Acta Mechanica Sinica,* **30**(1), pp. 73–83.

[333] Chen, Z., and Bobaru, F., 2015. "Peridynamic modeling of pitting corrosion damage". *Journal of the Mechanics and Physics of Solids,* **78**, pp. 352–381.

[334] Rokkam, S., Phan, N., Gunzburger, M., Shanbhag, S., and Goel, K., 2018. "Meshless peridynamics method for modeling corrosion crack propagation". In 6th International Conference on Crack Paths (CP 2018)(Verona, Italy). http://www. cp2018. unipr. it.

[335] Jafarzadeh, S., Chen, Z., and Bobaru, F., 2018. "Peridynamic modeling of intergranular corrosion damage". *Journal of The Electrochemical Society,* **165**(7), pp. C362–C374.

[336] Wilson, Z. A., and Landis, C. M., 2016. "Phase-field modeling of hydraulic fracture". *Journal of the Mechanics and Physics of Solids,* **96**, pp. 264–290.

[337] Heider, Y., and Markert, B., 2017. "A phase-field modeling approach of hydraulic fracture in saturated porous media". *Mechanics Research Communications,* **80**, pp. 38–46.

[338] Ehlers, W., and Luo, C., 2017. "A phase-field approach embedded in the theory of porous media for the description of dynamic hydraulic fracturing". *Computer Methods in Applied Mechanics and Engineering,* **315**, pp. 348–368.

[339] Zhou, S., Zhuang, X., and Rabczuk, T., 2019. "Phase-field modeling of fluid-driven dynamic cracking in porous media". *Computer Methods in Applied Mechanics and Engineering,* **350**, pp. 169 – 198.

[340] Wick, T., 2016. "Coupling fluid-structure interaction with phase-field fracture". *Journal of Computational Physics,* **327**, pp. 67 – 96.

[341] Wang, H., and Tian, H., 2012. "A fast galerkin method with efficient matrix assembly and storage for a peridynamic model". *Journal of Computational Physics,* **231**(23), pp. 7730–7738.

[342] Prakash, N., and Stewart, R. J., 2020. "A multithreaded method to assemble a sparse stiffness matrix for quasi-static solutions of linearized bond-based peridynamics". *Journal of Peridynamics and Nonlocal Modeling*, pp. 1–35.

[343] Cassell, A., and Hobbs, R., 1976. "Numerical stability of dynamic relaxation analysis of non-linear structures". *International Journal for numerical methods in engineering,* **10**(6), pp. 1407–1410.

[344] Topping, B., and Khan, A., 1994. "Parallel computation schemes for dynamic relaxation". *Engineering computations,* **11**(6), pp. 513–548.

[345] Kilic, B., and Madenci, E., 2010. "An adaptive dynamic relaxation method for quasi-static simulations using the peridynamic theory". *Theoretical and Applied Fracture Mechanics,* **53**(3), pp. 194–204.

[346] Shiihara, Y., Tanaka, S., and Yoshikawa, N., 2019. "Fast quasi-implicit nosb peridynamic simulation based on fire algorithm". *Mechanical Engineering Journal,* **6**(3), pp. 18–00363.

[347] Bitzek, E., Koskinen, P., Gähler, F., Moseler, M., and Gumbsch, P., 2006. "Structural relaxation made simple". *Physical review letters,* **97**(17), p. 170201.

[348] Saad, Y., and Schultz, M. H., 1986. "Gmres: A generalized minimal residual algorithm for solving nonsymmetric linear systems". *SIAM Journal on scientific and statistical computing,* **7**(3), pp. 856–869.

[349] Arnoldi, W., 1951. "The principle of minimized iteration in the solution of the matrix eigenvafue problem,". *Quart. Appl. Math,* **9**, pp. 17–29.

[350] Saad, Y., 1981. "Krylov subspace methods for solving large unsymmetric linear systems". *Mathematics of computation,* **37**(155), pp. 105–126.

[351] Nguyen, N.-H., Nguyen, V. P., Wu, J.-Y., Le, T.-H.-H., Ding, Y., et al., 2019. "Mesh-based and meshfree reduced order phase-field models for brittle fracture: One dimensional problems". *Materials,* **12**(11), p. 1858.

[352] Kerfriden, P., Goury, O., Rabczuk, T., and Bordas, S. P.-A., 2013. "A partitioned model order reduction approach to rationalise computational expenses in nonlinear fracture mechanics". *Computer methods in applied mechanics and engineering,* **256**, pp. 169–188.

[353] Kane, C., Marsden, J. E., and Ortiz, M., 1999. "Symplectic-energy-momentum preserving variational integrators". *Journal of mathematical physics,* **40**(7), pp. 3353–3371.

[354] Geelen, R., Plews, J., Tupek, M., and Dolbow, J., 2020. "An extended/generalized phase-field finite element method for crack growth with global-local enrichment". *International Journal for Numerical Methods in Engineering,* **121**(11), pp. 2534–2557.

[355] Ouchi, H., Katiyar, A., Foster, J. T., Sharma, M. M., et al., 2017. "A peridynamics model for the propagation of hydraulic fractures in naturally fractured reservoirs". *SPE Journal,* **22**(04), pp. 1–082.

[356] Ni, T., Zaccariotto, M., Zhu, Q.-Z., and Galvanetto, U., 2019. "Coupling of fem and ordinary state-based peridynamics for brittle failure analysis in 3d". *Mechanics of Advanced Materials and Structures*, pp. 1–16.

[357] Bobaru, F., and Silling, S. A., 2004. "Peridynamic 3d models of nanofiber networks and carbon nanotube-reinforced composites". In AIP Conference Proceedings, Vol. 712, American Institute of Physics, pp. 1565–1570.

[358] Jafarzadeh, S., Chen, Z., Zhao, J., and Bobaru, F., 2019. "Pitting, lacy covers, and pit merger in stainless steel: 3d peridynamic models". *Corrosion Science,* **150**, pp. 17–31.

[359] Bobaru, F., Ha, Y. D., and Hu, W., 2012. "Damage progression from impact in layered glass modeled with peridynamics". *Central European Journal of Engineering,* **2**(4), pp. 551–561.

[360] Hu, W., Wang, Y., Yu, J., Yen, C.-F., and Bobaru, F., 2013. "Impact damage on a thin glass plate with a thin polycarbonate backing". *International Journal of Impact Engineering,* **62**, pp. 152–165.

[361] Breitenfeld, M., 2014. "Quasi-static non-ordinary state-based peridynamics for the modeling of 3d fracture". PhD thesis, University of Illinois at Urbana-Champaign.

[362] Liu, W., and Hong, J.-W., 2012. "Discretized peridynamics for brittle and ductile solids". *International journal for numerical methods in engineering,* **89**(8), pp. 1028–1046.

[363] Dally, T., and Weinberg, K., 2017. "The phase-field approach as a tool for experimental validations in fracture mechanics". *Continuum Mechanics and Thermodynamics,* **29**(4), pp. 947–956.

[364] Noii, N., and Wick, T., 2019. "A phase-field description for pressurized and non-isothermal propagating fractures". *Computer Methods in Applied Mechanics and Engineering,* **351**, pp. 860 – 890.

[365] Weinberg, K., Dally, T., Schuß, S., Werner, M., and Bilgen, C., 2016. "Modeling and numerical simulation of crack growth and damage with a phase field approach". *GAMM-Mitteilungen,* **39**(1), pp. 55–77.

[366] Agwai, A., Guven, I., and Madenci, E., 2011. "Predicting crack propagation with peridynamics: a comparative study". *International journal of fracture,* **171**(1), p. 65.

[367] Ha, Y. D., and Bobaru, F., 2010. "Studies of dynamic crack propagation and crack branching with peridynamics". *International Journal of Fracture,* **162**(1-2), pp. 229–244.

[368] Agrawal, V., and Dayal, K., 2017. "Dependence of equilibrium griffith surface energy on crack speed in phase-field models for fracture coupled to elastodynamics". *International Journal of Fracture,* **207**(2), pp. 243–249.

[369] Yoshioka, K., Naumov, D., and Kolditz, O., 2020. "On crack opening computation in variational phase-field models for fracture". *Computer Methods in Applied Mechanics and Engineering,* **369**, p. 113210.

[370] Diehl, P., Tabiai, I., Baumann, F. W., Therriault, D., and Levesque, M., 2018. "Long term availability of raw experimental data in experimental fracture mechanics". *Engineering Fracture Mechanics,* **197**, pp. 21–26.

[371] Spetz, A., Denzer, R., Tudisco, E., and Dahlblom, O., 2020. "Phase-field fracture modelling of crack nucleation and propagation in porous rock". *International Journal of Fracture,* **224**, pp. 31–46.

[372] Silling, S. A., Weckner, O., Askari, E., and Bobaru, F., 2010. "Crack nucleation in a peridynamic solid". *International Journal of Fracture,* **162**(1-2), pp. 219–227.

[373] Littlewood, D. J., 2011. "A nonlocal approach to modeling crack nucleation in aa 7075-t651". In ASME International Mechanical Engineering Congress and Exposition, Vol. 54945, pp. 567–576.

[374] Niazi, S., Chen, Z., and Bobaru, F., 2020. "Crack nucleation in brittle and quasi-brittle materials: A peridynamic analysis".

[375] Bang, D., and Madenci, E., 2017. "Peridynamic modeling of hyperelastic membrane deformation". *Journal of Engineering Materials and Technology,* **139**(3).

[376] Waxman, R., and Guven, I., 2020. "Implementation of a neo-hookean material model in state-based peridynamics to represent nylon bead behavior during high-speed impact". In AIAA Scitech 2020 Forum, p. 0725.

[377] Ogden, R. W., 1997. *Non-linear elastic deformations*. Courier Corporation.

[378] Rivlin, R., 1948. "Large elastic deformations of isotropic materials iv. further developments of the general theory". *Philosophical Transactions of the Royal Society of London. Series A, Mathematical and Physical Sciences,* **241**(835), pp. 379–397.

[379] Ahadi, A., and Melin, S., 2018. "Capturing nanoscale effects by peridynamics". *Mechanics of Advanced Materials and Structures,* **25**(13), pp. 1115–1120.

[380] Bitzek, E., Kermode, J. R., and Gumbsch, P., 2015. "Atomistic aspects of fracture". *International Journal of Fracture,* **191**, pp. 13–30.

[381] Patil, S. P., Heider, Y., Padilla, C. A. H., Cruz-Chú, E. R., and Markert, B., 2016. "A comparative molecular dynamics-phase-field modeling approach to brittle fracture". *Computer Methods in Applied Mechanics and Engineering,* **312**, pp. 117–129.

[382] Buehler, M. J., 2008. *Atomistic Modeling of Materials Failure*. Springer.

[383] Du, Q., 2016. "Nonlocal calculus of variations and well-posedness of peridynamics". In *Handbook of peridynamic modeling*. Chapman and Hall/CRC, pp. 101–124.

[384] Gu, X., Madenci, E., and Zhang, Q., 2018. "Revisit of non-ordinary state-based peridynamics". *Engineering Fracture Mechanics,* **190**, pp. 31–52.

[385] Madenci, E., Dorduncu, M., Barut, A., and Phan, N., 2018. "A state-based peridynamic analysis in a finite element framework". *Engineering Fracture Mechanics,* **195**, pp. 104–128.

[386] Madenci, E., Dorduncu, M., Barut, A., and Phan, N., 2018. "Weak form of peridynamics for nonlocal essential and natural boundary conditions". *Computer Methods in Applied Mechanics and Engineering,* **337**, pp. 598–631.

[387] Prudhomme, S., and Diehl, P., 2020. "On the treatment of boundary conditions for bond-based peridynamic models". *Computer Methods in Applied Mechanics and Engineering,* **372**, p. 113391.

[388] D'Elia, M., Li, X., Seleson, P., Tian, X., and Yu, Y., 2019. "A review of local-to-nonlocal coupling methods in nonlocal diffusion and nonlocal mechanics". *arXiv preprint arXiv:1912.06668*.

[389] Silling, S. A., 2011. "A coarsening method for linear peridynamics". *International Journal for Multiscale Computational Engineering,* **9**(6).

[390] Delorme, R., Diehl, P., Tabiai, I., Lebel, L. L., and Lévesque, M., 2020. "Extracting constitutive mechanical parameters in linear elasticity using the virtual fields method within the ordinary state-based peridynamic framework". *Journal of Peridynamics and Nonlocal Modeling*, pp. 1–25.

[391] Yolum, U., Taştan, A., and Güler, M. A., 2016. "A peridynamic model for ductile fracture of moderately thick plates". *Procedia Structural Integrity,* **2**, pp. 3713–3720.

[392] Conradie, J., Becker, T., and Turner, D., 2019. "Peridynamic approach to predict ductile and mixed-mode failure". *R&D Journal,* **35**, pp. 1–8.

[393] Behzadinasab, M., 2019. "Peridynamic modeling of large deformation and ductile fracture". PhD thesis, UT Austin.

[394] Biner, S., and Hu, S. Y., 2009. "Simulation of damage evolution in composites: a phase-field model". *Acta materialia,* **57**(7), pp. 2088–2097.

[395] Doan, D. H., Bui, T. Q., Duc, N. D., and Fushinobu, K., 2016. "Hybrid phase field simulation of dynamic crack propagation in functionally graded glass-filled epoxy". *Composites Part B: Engineering,* **99**, pp. 266–276.

[396] Feng, D.-C., and Wu, J.-Y., 2018. "Phase-field regularized cohesive zone model (czm) and size effect of concrete". *Engineering Fracture Mechanics,* **197**, pp. 66–79.

[397] Yang, Z.-J., Li, B.-B., and Wu, J.-Y., 2019. "X-ray computed tomography images based phase-field modeling of mesoscopic failure in concrete". *Engineering Fracture Mechanics,* **208**, pp. 151–170.

[398] Nguyen, V. P., and Wu, J.-Y., 2018. "Modeling dynamic fracture of solids with a phase-field regularized cohesive zone model". *Computer Methods in Applied Mechanics and Engineering,* **340**, pp. 1000–1022.

[399] Santillán, D., Mosquera, J. C., and Cueto-Felgueroso, L., 2017. "Phase-field model for brittle fracture. validation with experimental results and extension to dam engineering problems". *Engineering Fracture Mechanics,* **178**, pp. 109–125.

[400] Bourdin, B., 1999. "Image segmentation with a finite element method". *Mathematical Modelling and Numerical Analysis,* **33**(2), pp. 229–244.

[401] Feng, X., and Prohl, A., 2003. "Numerical analysis of the Allen-Cahn equation and approximation for mean curvature flows". *Numerische Mathematik,* **94**, pp. 33–65.

[402] Feng, X., and Prohl, A., 2004. "Analysis of a Fully Discrete Finite Element Method for the Phase Field Model and Approximation of Its Sharp Interface Limits". *Math. Comp.,* **73**, pp. 541–567.